The Prevalence and Significance of Offset Magma Reservoirs at Arc Volcanoes

Allan H. Lerner[1*], Daniel O'Hara[1], Leif Karlstrom[1], Susanna K. Ebmeier[2], Kyle R. Anderson[3], Shaul Hurwitz[3]

[1]Department of Earth Sciences, University of Oregon, Oregon 97403, USA. [2]School of Earth & Environment, University of Leeds, Leeds LS2 9JT, UK. [3]U.S. Geological Survey, Moffett Field, California 94035, USA

Corresponding author: Allan Lerner (alerner@uoregon.edu)

Key Points:

- Geophysical imaging suggest that magma reservoirs are often significantly laterally offset from overlying arc volcanoes
- Offset magma reservoirs are more prevalent at small volcanoes, whereas larger volcanoes have more centrally aligned magma storage
- Characterizing edifice topography may help predict subsurface magma storage geometries and guide volcano monitoring networks

Abstract

Determining the spatial relations between volcanic edifices and their underlying magma storage zones is fundamental for characterizing long-term evolution and short-term unrest. We compile centroid locations of upper crustal magma reservoirs at 56 arc volcanoes inferred from seismic, magnetotelluric, and geodetic studies. We show that magma reservoirs are often horizontally offset from their associated volcanic edifices by multiple kilometers, and the degree of offset broadly scales with reservoir depth. Approximately 20% of inferred magma reservoir centroids occur outside of the overlying volcano's mean radius. Furthermore, reservoir offset is inversely correlated with edifice size. Taking edifice volume as a proxy for long-term magmatic flux, we suggest that high flux or prolonged magmatism leads to more centralized magma storage beneath arc volcanoes by overprinting upper crustal heterogeneities that would otherwise affect magma ascent. Edifice volumes therefore reflect the spatial distribution of underlying magma storage, which could help guide monitoring strategies at volcanoes.

Plain Language Summary

Magma reservoirs are commonly assumed to be located directly beneath their associated volcanic edifices. This "central reservoir" paradigm dominates volcano modeling and monitoring. However, the actual spatial relations between volcanoes and underlying magma reservoirs are poorly known. We compile a database of geophysical studies at subduction zone volcanoes where magma reservoirs were detected through subsurface modeling of seismic waves and ground deformation. We then systematically map volcano shapes and compare their center locations with associated magma reservoirs. We find that while the majority of volcanic systems are centralized, a substantial number of volcanoes have magma reservoirs laterally offset multiple kilometers from their volcano's centers. Approximately 20% of magma reservoirs are located beyond the edifice radii, or outside the "footprints" of their volcanoes. Additionally, magma reservoirs are more laterally offset at small volcanoes, but more centrally aligned at large volcanoes. We propose that increased magma flux at large volcanoes thermally overprints crustal faults and heterogeneities, leading to progressively more centrally focused magmatic systems. Our work suggests that the central reservoir view of volcanic systems should be revised to account for magma focusing as volcanoes grow. Recognizing the global prevalence of laterally offset magmatic systems may better help design volcano monitoring networks.

1 Introduction

Volcano monitoring strategies and models of magma transport in the shallow crust often implicitly assume that magma storage occurs directly under topographic highs of the volcanoes they feed (Moran et al., 2008; Pinel & Jaupart, 2003; Sparks et al., 2012). With an increasing quantity and quality of seismic and magnetotelluric (MT) data, it has been recognized that some magmatic storage zones (hereafter "magma reservoirs") are laterally offset from their associated volcanic edifices (Aizawa et al., 2014; Syracuse et al., 2015; Vargas et al., 2017). Geodetic observations have similarly demonstrated that a substantial proportion of deformation signals occur relatively distant to volcanic edifices (Lu & Dzurisin, 2014; Ebmeier et al., 2018). Lateral offsets are also commonly observed at analog systems such as geysers (Hurwitz & Manga,

2017). However, a systematic compilation and study of offset magma reservoirs at volcanic systems is lacking.

The best available means to assess the locations of magma reservoirs at volcanoes is through geophysical imaging techniques such as seismic and MT tomography, and from inversion of geodetic data. Seismic tomography measures variations in seismic velocities arising from spatially varying lithology, fluid and melt fraction, temperature, and crystallographic alignment (Lees, 2007). MT is sensitive to properties controlling electrical conductivity, namely fluid fraction, melt fraction, lithology/fluid composition, and fluid connectivity (Chave & Jones, 2012). Geodesy (e.g., InSAR, GPS, leveling) measures displacement of the ground surface due to processes such as magma injection or withdrawal, cooling and crystallization of magma bodies, accumulation of magmatic gases, or pressure changes in shallow hydrothermal systems (Dzurisin & Lu, 2007). These techniques are thus sensitive to different, but contemporaneous, aspects of subsurface magma storage and transport.

Quantifying the global pervasiveness of laterally offset magma reservoirs and their depth distributions relative to volcanic edifice volumes and morphologies (Castruccio et al., 2017; Pinel & Jaupart, 2003), magma compositions and degassing rates (Wallace, 2005), stress states of volcanic arcs (Chaussard & Amelung, 2012; Pinel & Jaupart, 2000) and host rock lithologies (Maccaferri et al., 2011; Taisne & Jaupart, 2009) is critical for identifying the key physical processes that control magma transport in the upper crust. In order to address such questions, we compile a database containing topographic characterizations of volcanic edifices and of geophysically inferred subsurface locations of associated magma reservoirs. We restrict our study to arc volcanoes to limit the potential tectonic variability of hotspot and rift systems. The high threat of many arc volcanoes further motivates the need to better understand these systems.

2 Methods

2.1 Database of geophysically inferred magma reservoir locations

We include in our database magma storage locations from studies published between 2000 and 2018 in which authors explicitly locate a reservoir at depths of 2.5 to 15 km below the local mean ground surface, and where the spatial resolution is sufficiently high (kilometers-scale). Shallower reservoirs are excluded to avoid the preponderance of hydrothermal features, which are difficult to distinguish from magmatic features using geophysical methods. This necessarily excludes a number of published studies, but the resulting database still contains 77 inferred magma reservoirs at 56 arc volcanoes. Forty-seven reservoirs are from geodetic inversions and 30 are inferred from seismic and/or MT tomographic models (Figure 1). Owing to the challenges of maintaining consistency between the diverse datasets, we utilize only the magma reservoir centroid positions (latitude, longitude, and depth of the center of tomographic anomalies and modelled deformation sources) rather than attempting to identify the geometry and spatial extent of magma storage. While tomography can identify crustal anomalies with low seismic velocities or high electrical conductivities that may be related to either dynamic or static magma reservoirs, geodetic signals indicate active magmatic processes. Therefore, the centroid of a modelled deformation source is not necessarily the center of a magma reservoir, but rather a region where detectable deformation at depth (commonly attributed to pressure changes) is occurring. Conversely, magmatic tomographic anomalies do not necessarily imply potentially

mobile magma, as there is seldom sufficient resolution to identify particular areas of high melt concentration.

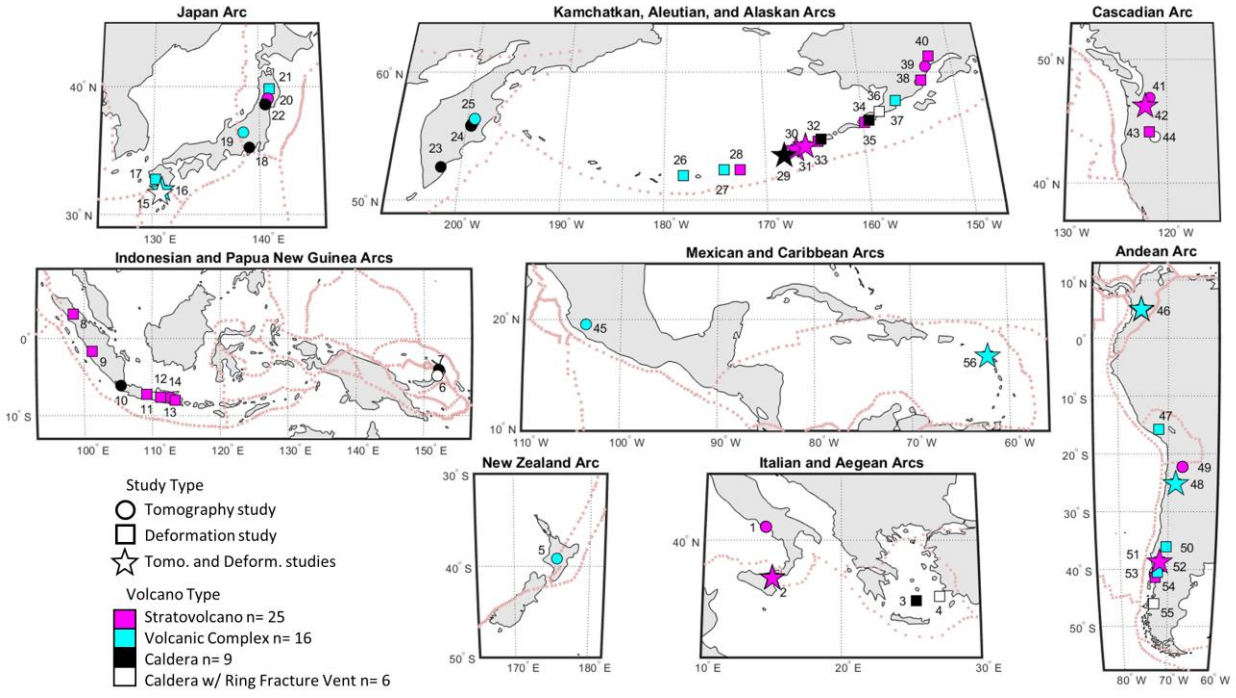

Figure 1. Global distribution of arc volcanoes with geophysically inferred magma reservoirs used in this study. Symbol colors indicate volcanic edifice type and symbol shapes indicates the type of geophysical method. Plate boundaries are mapped in red dashed lines. Volcano numbers relate to information in Tables S1, S2 and Figure S1.

2.2 Coupling geophysical observations with surface topography

Assessing the spatial relation between magma reservoirs and associated volcanic landforms requires a consistent method of characterizing volcanic edifice topography. Most volcanoes are constructed through repeated, localized eruptions and intrusions so that overall volcanic edifice size and shape is a better indicator of the time-averaged locus of volcanic output than the location of an individual vent or volcanic peak. We therefore examine the spatial relations between edifice centroids (the geometrical center of topography, largely determined by low-lying basal area) and magma reservoir centroids. In topographically complicated volcanic settings with flank or nested vents and domes, or where vents have formed along caldera-bounding faults, we consider features of similar age and petrologic character (chemical and isotopic compositions) to be related as an overall volcanic complex. We then treat each complex as a single edifice. Often there is an age progression of structures within volcanic complexes or post-caldera eruptive features, so in viewing volcanic complexes as single edifices we are effectively using a longer timeframe to define the surface expression of a volcanic system. We therefore classify some volcanoes differently than in the Smithsonian Institution database (2013) (Text S2, Tables S1, S2).

We characterize the topography of each edifice using a closed contour algorithm (Bohnenstiehl et al., 2012), which fits an adjusted basal contour around a volcano, accounting for background slope and the presence of nearby topographic features. Once the bounds of an edifice are defined, the volume, relief, mean radius, and topographic centroid are calculated (Text S2). This method generally produces a conservative estimate of basal contour and therefore edifice volume. By using this mapping algorithm, coupled with a global 30 m digital elevation model (DEM) (NASA JPL, 2013) and a bathymetry database for subaqueous locations (Amante & Eakins, 2009), we maintain a consistent approach for quantifying edifice geometry.

Based on geophysical data quality (e.g., number of stations, ray path coverage, duration of measurement, goodness of model fits, author-stated confidence) and corroborating datasets (earthquake locations, petrologic geobarometry, observed co-eruptive linkages between reservoir locations and edifices), we assign confidence values of low, high, and near-certain (reservoirs with co-eruptive links to edifices) to reservoir locations and to their associations with particular volcanoes. Mount St. Helens (USA) provides an example where the location of the syn-eruptive deformation source is consistent with earthquake locations, leading to high confidence in the modelled geodetic source location and connection to the edifice (Figure 2a). In comparison, a reservoir location to the southwest of the volcano that is inferred from seismic tomography does not share such evidence and is assigned a lower confidence factor. However, filtering the dataset by this confidence value does not greatly affect the results. A more extensive discussion of methods, data sources, and assessment of confidence is presented in supplemental text S1 – S4. Edifice and magma reservoir location parameters can be found in data sets S1 (edifice bounds maps) and S2 (Google Earth database).

3 Results and Discussion

3.1 Distribution of magma reservoirs beneath arc volcanoes

We define reservoir "lateral offset" as the horizontal distance from a magma reservoir centroid to an associated volcanic edifice centroid (Figure 2a). As the spatial scale of volcanic edifices varies widely (mean radii range from 2 to 16 km), it is also useful to define reservoir "scaled offset" as the magma reservoir lateral offset relative to the mean edifice radius (Figure 3). Considering these metrics, we find the following relations:

3.1.1 Central and offset reservoirs

Although the majority of magma reservoir centroids underlie their respective edifices, more than one third (34%) are offset by ≥ 4 km from their edifice centroids (Figure 2b, Table S3, Figure S5). 18% of the reservoir centroids are outside the "footprint" of their associated edifice, defined as > 1 mean radius distance from the edifice centroid (Figure 3). Basalt-dominated systems have somewhat more centrally aligned reservoirs compared to more silicic volcanoes (Figures S9, S15). The degree of reservoir offset has no apparent relation to arc stress regime, subduction convergence direction, or SO_2 degassing rate (Figures S2, S3, S12, S13). Overall, magma reservoirs are slightly more aligned with edifice centroid locations than with recent eruptive vents or summit locations (Figures S8, S9).

3.1.2 Reservoir depths

Magma reservoirs occur throughout the entire 2.5 – 15 km depth range considered in the

dataset (Figure 2b). However, the sensitivity of geophysical techniques generally decreases with depth, so it is probable that deeper magma reservoirs are under-recorded. Noting this caveat, we find that magma reservoirs in the full dataset have a mean depth of 7.4 ± 3.4 km (6.9 km median). Reservoirs with observed co-eruptive links have a similarly large depth range of 7.1 ± 3.4 km (Table S3). Assuming an upper crustal density of 2.75 g/cm^3, the 7.4 ± 3.4 km mean depth of the full dataset translates to storage pressures of 2.0 ± 0.9 kbar. This pressure range encompasses most of the upper crust and is nearly double the range of magma storage pressures of 2.0 ± 0.5 kbar proposed by Huber et al. (2019). Within the granularity of our compilation, volcanoes with dacitic and rhyolitic compositions tend to have shallower reservoirs than more mafic systems (Figures S9, S16). We find no apparent correlation between reservoir depth and the regional stress regime, in contrast to previous interpretations (Chaussard & Amelung, 2012) (Figure S2).

Larger lateral offsets are more commonly observed when magma reservoirs are deeper (Figure 2b): 49% (n=38) of reservoirs occur within an area beneath edifices defined by the 1:2 slope of offset to reservoir depth, whereas 83% (n= 64) occur within a 1:1 contour and 99% (n=77) occur within a 2:1 contour. This implies a distributed catchment area for rising magma beneath edifices (Ebmeier et al., 2018; Karlstrom et al., 2009). Arc volcanoes with calderas are more commonly associated with shallower, central magma reservoirs (Figure 2b, Figures S15, S16), consistent with models of collapse calderas involving relatively shallow evacuated magma reservoirs (Acocella, 2007; Lipman, 1997). Geophysical observations of many calderas with ring fracture vents in the database suggest the presence of multiple reservoirs, typically with a shallow reservoir close to the post-caldera ring fracture vent and a deeper reservoir more centrally located under the caldera (Tables S1, S2).

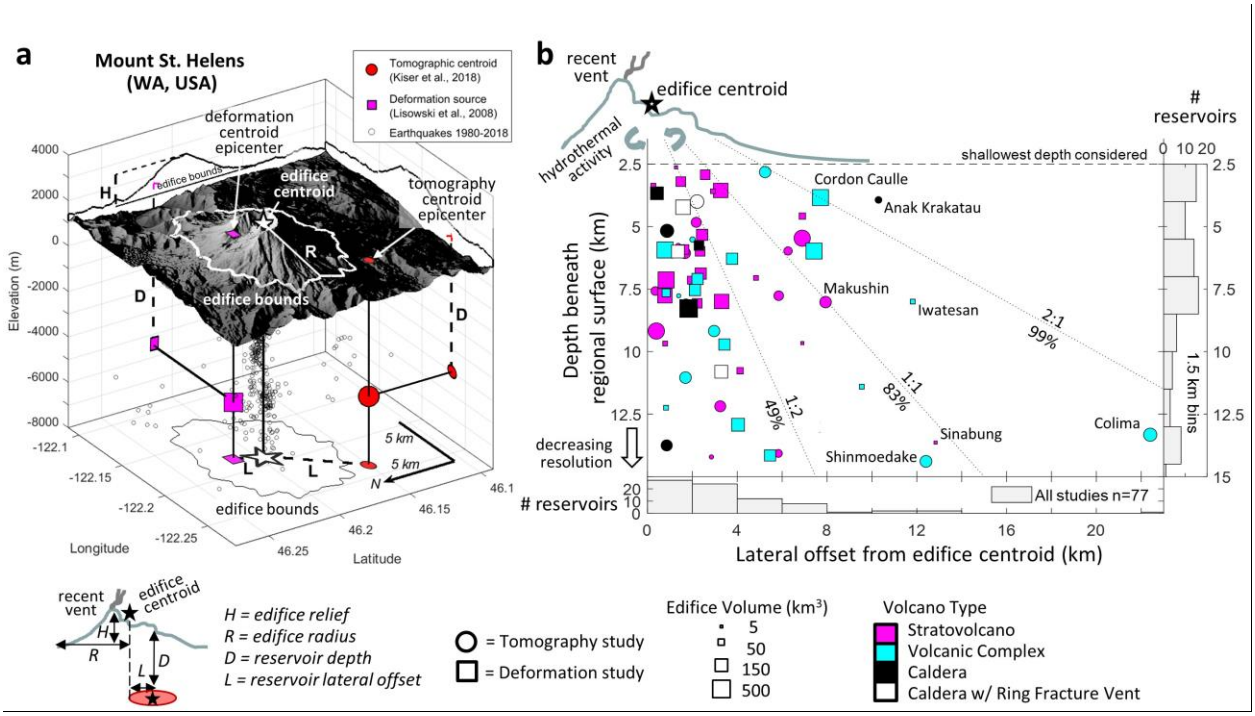

Figure 2. ***(a)*** Inferred magma reservoir locations and the volcanic edifice of Mount St. Helens, with the key parameters used in this study labeled. Edifice bounds calculated from surface topography (measured February 2000) are shown in white and projected to the figure base, the star is the calculated edifice centroid, *R* denotes the mean edifice radius from the centroid, and *H* is edifice height. The centroids of magma reservoirs are inferred from seismic tomography (Kiser et al., 2018) and from co-eruptive deformation between 2004 and 2006 (Lisowski et al., 2008). *L* is the lateral offset of magma reservoir centroid from edifice centroid, *D* is magma reservoir centroid depth relative to local surface elevation (Text S1, S3). Earthquake locations for reviewed events larger than magnitude 1 between 1980 and 2018 are shown for context (n = 10508; Pacific Northwest Seismic Network) (University of Washington, 1963). ***(b)*** Lateral offset and depth distribution of magma reservoir centroids relative to their associated volcanic edifices for the global dataset. The percentages of magma reservoirs occurring within different lateral offset to depth ratios are shown. Symbols are classified by volcano type (color), and whether the magma reservoirs were inferred tomographically (circles) or geodetically (squares). Symbol size scales with edifice volume. Thirteen magma reservoirs at volcanoes with unquantified edifice volumes are included in the vertical and horizontal histograms but are not shown in the main plot.

3.2 Relations between magma reservoir locations and edifice volumes

We find that magma reservoirs beneath smaller edifices are generally more offset, both in absolute and scaled distances (Figure 3a,b). Edifice volumes form a continuum over > 3 orders of magnitude (Grosse et al., 2014; Karlstrom et al., 2018), and range from 6 to 730 km^3 in our database, with a relatively continuous distribution (Figures S4, S14). At volcanoes with edifice volumes ≤ 43 km^3 (for reference, the volume of Mount St. Helens [Figure 2a]), 50% of reservoir centroids are located > 4 km from the edifice centroid (n=10 of 20), whereas only 23% of reservoir centroids at larger volcanoes are offset > 4 km (n=10 of 44). Similarly, 45% of reservoirs at volcanoes with edifice volumes ≤ 43 km^3 are laterally offset beyond their edifice radii (scaled offset > 1), but only 7% of reservoirs at larger volcanoes are offset to this degree (Figure 3a; Figure S5). Most volcanoes with reservoir scaled offsets > 1 are small volume andesitic stratovolcanoes or volcanic complexes (Figure S4). There are no notable differences in reservoir depths beneath small and large volcanoes within the upper 15 km of crust (Figure 2b, Figure S16), in contrast to some model predictions (Castruccio et al., 2017). Lastly, we note that magma reservoir locations inferred from tomographic models and from inversions of geodetic data conducted at the same volcano often differ substantially, diverging up to 4 – 10 km horizontally and 2 – 8 km vertically (Text S1, Figure S7). Such differences are likely a result of surface displacements being generated by pressure changes in only a part of a larger reservoir system, as well as differences in the sensitivities of the geophysical techniques (Dzurisin & Lu, 2007; Ebmeier et al., 2018; Lees, 2007).

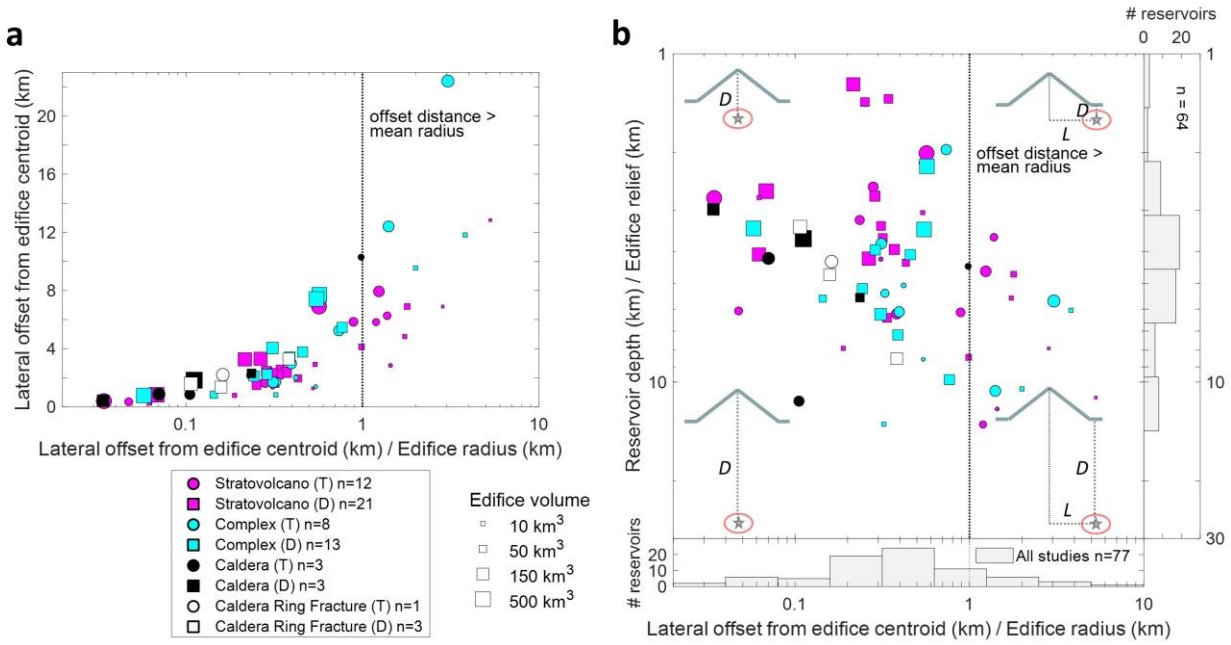

Figure 3. ***(a)*** Magma reservoir absolute offsets compared to scaled offsets. Edifice centroids with scaled offsets > 1 fall outside the "footprint" of the edifice. Most magma reservoirs with substantial absolute and scaled offsets occur under smaller volcanoes. ***(b)*** Non-dimensional view of reservoir offset relative to depth, showing that when scaled to edifice height and radius, magma reservoirs at smaller edifices are relatively deeper and more offset, as schematically depicted (*D* is depth; *L* is lateral offset). The database is limited to reservoirs between 2.5 and 15 km depth, which may explain the general lack of reservoirs in the lower left quadrant. Symbol shape, color, and size are as defined in Figure 2. *(T)* and *(D)* indicate tomography and deformation studies, respectively. Thirteen magma reservoirs at volcanoes with unquantified edifice volumes are included in the horizontal histogram but are not shown in the other plots.

3.3 Controls on magma reservoir geometry

The established relation between edifice volumes and the degree to which magma storage is located beneath arc volcanoes has significant implications for modeling magma transport and for volcano monitoring. For example, more laterally offset reservoirs at smaller volcanoes suggests that volcano size encodes some geometrical aspects of the subsurface transport network. Smaller volcanoes are indicative of low-flux or thermally immature systems with shorter histories of volcanic effusion. We infer that low-flux and/or young systems have less centralized magma storage and transport networks than systems with higher magma flux or longer durations of magmatic activity. Further, we propose that this observed relationship is related to a loss of crustal heterogeneity due to the degree of heating, changes to deviatoric stress, and lithologic replacement of host rock by magma intrusions (Figure 4). Such homogenization is a function of the magnitude and the duration of mass and heat input into the shallow crust (Annen & Sparks, 2002; Karlstrom et al., 2017). In systems with more limited magma flux into and through the shallow crust, pre-existing structural and stress heterogeneities may more significantly influence ascending magma. For example, horizontal or inclined faults (Galland et al., 2007) and lithologic

contacts (Magee et al., 2016) facilitate lateral magma transport and the development of laterally offset reservoirs, as do pre-existing background stresses (Maccaferri et al., 2011). Indeed, a number of volcanoes with laterally offset reservoirs occur near major crustal faults (Jay et al., 2014; Lundgren et al., 2015; White & McCausland, 2016).

In contrast, systems with a high magma flux and/or long histories of volcanism alter the shallow crust through cycles of repeated heating, stress changes and intrusion. Deviatoric stresses associated with transient magma storage and volcanic edifice loads may focus dike propagation (Maccaferri et al., 2011; Pinel & Jaupart, 2004; Roman & Jaupart, 2014) and concentrate heat at shallow depths beneath volcanoes. This transport eventually replaces the crustal column and establishes the lateral region of thermomechanically focused magma ascent beneath volcanoes. As crustal impediments to vertical dike ascent are overprinted, eruption locations may become more aligned with the underlying reservoir, causing the volcanic edifice position to progressively migrate. The load of this evolving edifice contributes to further focusing dike ascent, and the magma reservoir may similarly migrate in adjustment to the changing thermal state of the shallow crust (Figure 4b). We propose that, over time, these self-reinforcing mechanisms at high-flux magmatic systems result in larger volcanic edifices being centered above their magma storage zones.

The nature of mechanical coupling between edifice loads and magma reservoirs depends on the wavelength of edifice topography compared to reservoir depth. In the database, all reservoir centroid depths are within an order of magnitude of their edifice diameters (Figure S6), implying that the elastic stress and deformation fields associated with the edifice load and reservoir should interact (McTigue & Segall, 1988). Scaling reservoir depths by edifice relief, which sets the magnitude of the surface load, we find that reservoirs are generally deeper relative to the overlying edifice as they become more offset (Figure 3b), consistent with a distributary region of magma supply.

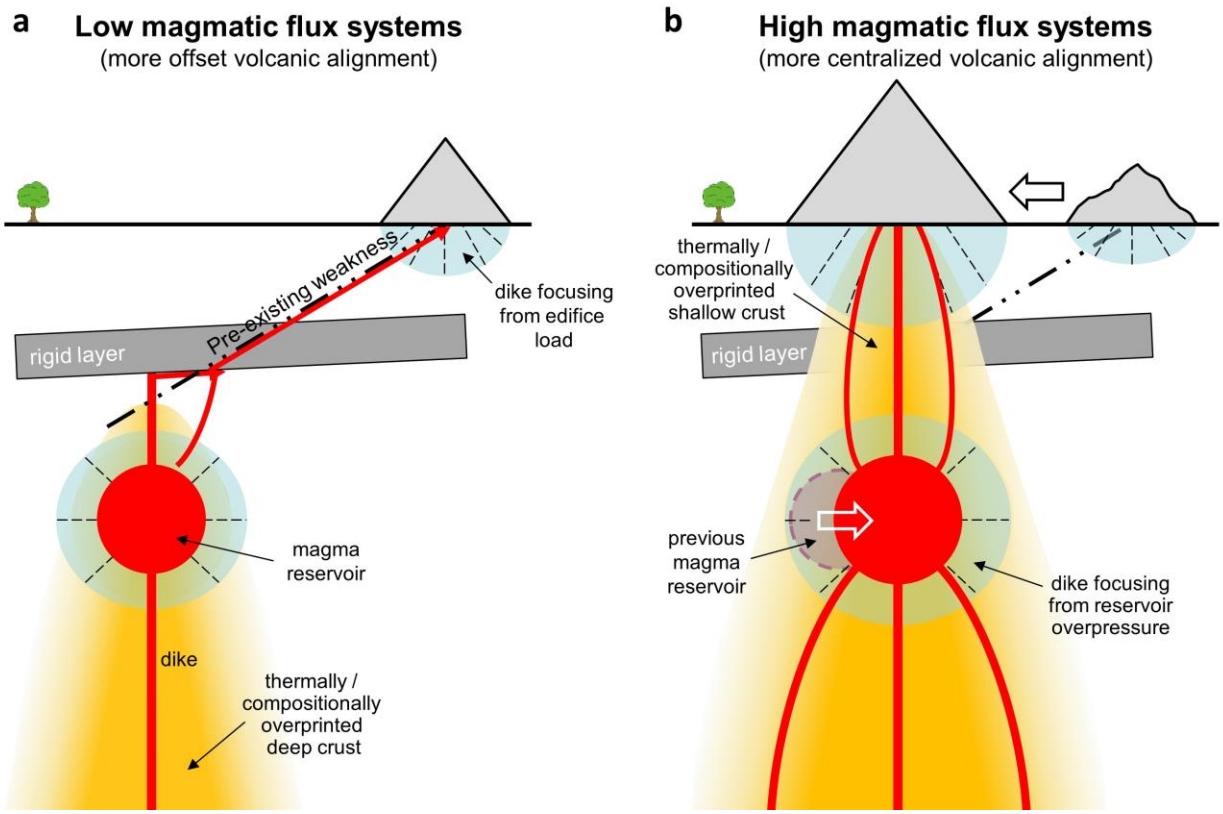

Figure 4. Schematic representation of a magma reservoir and transport system at low- and high-flux volcanoes. ***(a)*** Small volcanoes may be a consequence of low magnitude or short-lived magmatic flux. In low-flux systems, much of the upper crust retains heterogeneities that may cause increased lateral transport of magma along zones of weakness (e.g., rheologically competent strata blocking or diverting dike propagation to along faults or between lithologic contacts). ***(b)*** Large volcanoes reflect more long-lived or high-flux magmatic systems, which can overprint crustal heterogeneities leading to more focused vertical dike ascent. Magma reservoir locations may similarly migrate (white arrow) in response to changing edifice locations (large black arrow). These self-reinforcing processes can contribute to progressively more aligned volcanic systems through time.

3.4 Relevance for monitoring active volcanoes

With a simple determination of edifice shape from a DEM (radius, relief, centroid), we can estimate the lateral extent in which underlying shallow crustal reservoirs are likely to occur (Figures 2b and 3). This estimation can be further refined by quantifying edifice size, since large volcanoes are more likely to have centralized magmatic reservoirs compared with smaller volcanoes.

For example, Mt. Hood in Oregon (USA) is a high-threat andesitic stratovolcano (Ewert et al., 2018), but there are no constraints on the location of its magma reservoir(s). Based on the calculated edifice topography of Mt. Hood (2350 m relief, 6.5 km mean radius, 89 km^3 volume), and assuming a reservoir depth of 6 ± 2 km from geobarometry (Cooper & Kent, 2014), the relation presented in Figure 3b (with 80% prediction intervals; Figure S17) suggests that the

magma reservoir centroid is likely to be within 6 km of the edifice centroid (where the edifice centroid is ~1 km SE of the summit [Data Sets S1, S2]). In contrast, Mt. Bachelor (also in Oregon) is a smaller Holocene basaltic stratovolcano (900 m relief, 2.7 km mean radius, 8 km^3 volume) and may host a magma reservoir offset by up to 9 km from its edifice centroid, assuming a reservoir depth equal to the mean depth for basaltic reservoirs in the dataset (6.8 ± 2.4 km).

The relatively common occurrence of offset reservoirs warrants reassessing the design of monitoring networks at arc volcanoes. Focusing monitoring instruments exclusively on an edifice (or a particular eruptive vent) might miss early signs of unrest at offset systems (Ebmeier et al., 2018). Ground-based monitoring networks or satellite survey footprints may thus be planned more strategically based on simple characterization of the edifice topography. Barring *a priori* knowledge of subsurface magma reservoir geometry, monitoring coverage should be expanded at smaller volcanoes given their increased likelihood of being associated with more offset reservoirs. Additionally, as edifice centroids tend to be more aligned with magma reservoirs than recent eruptive vents or summits, focusing monitoring networks around edifice centroids rather than vent or summit locations might enable better detections of unrest.

Finally, laterally offset magma reservoirs require horizontal or inclined pathways of magma ascent to the surface (Aizawa et al., 2014; Aoki et al., 2013; Wicks et al., 2011). Non-vertical transport pathways are not commonly included in models for dike propagation and could alter interpretations of geophysical monitoring signals (Rivalta et al., 2015; White & McCausland, 2016). Inclined dikes may also facilitate fluid phase separation during transport, with implications for magmatic degassing and modeling of conduit dynamics (Massol et al., 2001; Vandemeulebrouck et al., 2014).

4 Conclusions and future research

By combining geophysical and volcanic landform topography datasets we have identified new constraints on the subsurface geometry of shallow arc magma transport. In particular, we find that magma reservoirs are commonly offset from the presumed volcanic edifices they source. We observe that laterally offset magma reservoirs are more prevalent at small volume volcanoes than at large volcanoes, and consequently propose that the magnitude and duration of magmatic flux influences the degree of vertical alignment between edifices and reservoirs. This hypothesis implies that shallow magma storage zones and volcanic edifice positions evolve through time to become large systems with well-developed, centrally aligned magma transport. The characterization of volcanic edifice topography thus informs the subsurface geometry of shallow magma storage, which may help guide the spatial design of volcano monitoring networks.

An improved ability to consistently constrain geometries and volumes of magma reservoirs would significantly build upon our analysis. For example, dikes may initiate from the edges of magmatic storage zones so that transport pathways could be located away from the centroids of large reservoirs. Further efforts to combine geophysical and topographic datasets from other arc and non-arc volcanoes, along with studies that constrain volcanic histories, will be required to validate the hypothesis that edifice growth corresponds to the centralization of magma transport. Integrating edifice topography and magma reservoir locations with local

tectonic features, substrate lithologies, durations of magmatism, and edifice growth and collapse histories has great potential for improving our understanding of the co-evolution of volcanic edifices and underlying magma storage and transport systems.

We hope the compilation and observations presented here motivate further efforts to *a)* expand and refine similar geophysical and topographic datasets at volcanoes worldwide, *b)* assess thermomechanical interactions between edifices and reservoirs to understand the origin and impacts of offset reservoirs, c*)* more routinely publish the centroids of major tomographic anomalies and pressure sources (with uncertainties) in future geophysical studies, and *d)* reconsider what criteria are used to define volcano locations (e.g., vents or edifice centroids), edifice boundaries, and volcano structures.

Acknowledgments, Samples, and Data

A.H.L. and D.O. acknowledge support from the National Science Foundation Graduate Research Fellowship Program under grant #1309047. L.K. acknowledges funding through NSF CAREER 1848554. S.K.E. is supported by a UKRI NERC Independent Research Fellowship and also acknowledges a European Space Agency Living Planet Fellowship and the NERC-BGS Centre for Observation and Modelling of Earthquakes, Volcanoes, and Tectonics (COMET). K.R.A. and S.H. were funded by the U.S. Geological Survey's Volcano Hazards Program. A.L. thanks the University of Oregon geophysics community for many fruitful discussions on tomography methodology and interpretation. We thank Mike Poland and two anonymous reviewers for constructive comments that significantly improved this manuscript, and thank Chris Huber for editorial handling. Any use of trade, firm, or product names is for descriptive purposes and does not imply endorsement by the U.S. Government. We declare no competing interests. Datasets for this research are openly available at https://doi.org/10.7910/DVN/LHD1HY (Lerner, 2020).

References

Acocella, V. (2007). Understanding caldera structure and development: An overview of analogue models compared to natural calderas. *Earth-Science Reviews*, *85*(3–4), 125–160.

Aizawa, K., Koyama, T., Hase, H., Uyeshima, M., Kanda, W., Utsugi, M., et al. (2014). Three-dimensional resistivity structure and magma plumbing system of the Kirishima Volcanoes as inferred from broadband magnetotelluric data. *Journal of Geophysical Research: Solid Earth*, *119*(1), 198–215.

Amante, C., & Eakins, B. W. (2009). ETOPO1 1 arc-minute global relief model procedures, data sources and analysis: NOAA Technical Memorandum NESDIS NGDC-24. *National Geophysical Data Center, NOAA*, *10*(V5C8276M).

Annen, C., & Sparks, R. S. J. (2002). Effects of repetitive emplacement of basaltic intrusions on thermal evolution and melt generation in the crust. *Earth and Planetary Science Letters*, *203*(3), 937–955. https://doi.org/10.1016/S0012-821X(02)00929-9

Aoki, Y., Takeo, M., Ohminato, T., Nagaoka, Y., & Nishida, K. (2013). Structural controls on

magma pathways beneath Asama Volcano, Japan. *Geol. Soc. London Spec. Publ*, *380*, 67–84.

Argus, D. F., Gordon, R. G., & DeMets, C. (2011). Geologically current motion of 56 plates relative to the no-net-rotation reference frame. *Geochemistry, Geophysics, Geosystems*, *12*(11).

Bohnenstiehl, D. R., Howell, J. K., White, S. M., & Hey, R. N. (2012). A modified basal outlining algorithm for identifying topographic highs from gridded elevation data, Part 1: Motivation and methods. *Computers & Geosciences*, *49*, 308–314.

Calvert, A. T., Fierstein, J., & Hildreth, W. (2018). Eruptive history of Middle Sister, Oregon Cascades, USA–Product of a late Pleistocene eruptive episode. *Geosphere*, *14*(5), 2118–2139.

Carn, S. A., Fioletov, V. E., McLinden, C. A., Li, C., & Krotkov, N. A. (2017). A decade of global volcanic SO 2 emissions measured from space. *Scientific Reports*, *7*, 44095.

Castruccio, A., Diez, M., & Gho, R. (2017). The influence of plumbing system structure on volcano dimensions and topography. *Journal of Geophysical Research: Solid Earth*, *122*(11), 8839–8859.

Chaussard, E., & Amelung, F. (2012). Precursory inflation of shallow magma reservoirs at west Sunda volcanoes detected by InSAR. *Geophysical Research Letters*, *39*(21). https://doi.org/10.1029/2012GL053817

Chave, A. D., & Jones, A. G. (2012). *The magnetotelluric method: Theory and practice*. Cambridge University Press.

Comeau, M. J., Unsworth, M. J., Ticona, F., & Sunagua, M. (2015). Magnetotelluric images of magma distribution beneath Volcán Uturuncu, Bolivia: Implications for magma dynamics. *Geology*, *43*(3), 243–246.

Cooper, K. M., & Kent, A. J. (2014). Rapid remobilization of magmatic crystals kept in cold storage. *Nature*, *506*(7489), 480–483.

Dzurisin, D., & Lu, Z. (2007). Interferometric synthetic-aperture radar (InSAR). In *Volcano Deformation* (pp. 153–194). Springer.

Ebmeier, S. K., Andrews, B. J., Araya, M. C., Arnold, D. W. D., Biggs, J., Cooper, C., Cottrell, E., Furtney, M., Hickey, J., Jay, J., et al. (2018). Synthesis of global satellite observations of magmatic and volcanic deformation: implications for volcano monitoring & the lateral extent of magmatic domains. *Journal of Applied Volcanology*, *7*(1), 2. https://doi.org/10.1186/s13617-018-0071-3

Ewert, J. W., Diefenbach, A. K., & Ramsey, D. W. (2018). *2018 update to the U.S. Geological Survey national volcanic threat assessment*. U.S. Geological Survey Scientific Investigations Report 2018–5140, 40 p., https://doi.org/10.3133/ sir20185140.

Flusser, J., Suk, T., & Zitová, B. (2016). *2D and 3D image analysis by moments*. John Wiley & Sons.

Fournier, R. O. (1999). Hydrothermal processes related to movement of fluid from plastic into brittle rock in the magmatic-epithermal environment. *Economic Geology*, *94*(8), 1193–1211. https://doi.org/10.2113/gsecongeo.94.8.1193

Galland, O., Cobbold, P. R., de Bremond d'Ars, J., & Hallot, E. (2007). Rise and emplacement of magma during horizontal shortening of the brittle crust: Insights from experimental modeling. *Journal of Geophysical Research: Solid Earth*, *112*(B6). https://doi.org/10.1029/2006JB004604

Grosse, P., Euillades, P. A., Euillades, L. D., & de Vries, B. van W. (2014). A global database of composite volcano morphometry. *Bulletin of Volcanology*, *76*(1), 1–16.

Heuret, A., & Lallemand, S. (2005). Plate motions, slab dynamics and back-arc deformation. *Physics of the Earth and Planetary Interiors*, *149*(1–2), 31–51.

Hildreth, W. (2007). *Quaternary magmatism in the Cascades: Geologic perspectives*. US Geological Survey.

Hill, G. J., Bibby, H. M., Ogawa, Y., Wallin, E. L., Bennie, S. L., Caldwell, T. G., et al. (2015). Structure of the Tongariro Volcanic system: Insights from magnetotelluric imaging. *Earth and Planetary Science Letters*, *432*, 115–125.

Huber, C., Townsend, M., Degruyter, W., & Bachmann, O. (2019). Optimal depth of subvolcanic magma chamber growth controlled by volatiles and crust rheology. *Nature Geoscience*, 1–7.

Hurwitz, S., & Manga, M. (2017). The fascinating and complex dynamics of geyser eruptions. *Annual Review of Earth and Planetary Sciences*, *45*, 31–59.

Jaxybulatov, K., Koulakov, I., Ibs-von Seht, M., Klinge, K., Reichert, C., Dahren, B., & Troll, V. R. (2011). Evidence for high fluid/melt content beneath Krakatau volcano (Indonesia) from local earthquake tomography. *Journal of Volcanology and Geothermal Research*, *206*(3), 96–105.

Jay, J., Costa, F., Pritchard, M., Lara, L., Singer, B., & Herrin, J. (2014). Locating magma reservoirs using InSAR and petrology before and during the 2011–2012 Cordón Caulle silicic eruption. *Earth and Planetary Science Letters*, *395*, 254–266.

Karlstrom, L., Dufek, J., & Manga, M. (2009). Organization of volcanic plumbing through magmatic lensing by magma chambers and volcanic loads. *Journal of Geophysical Research: Solid Earth*, *114*(B10). https://doi.org/10.1029/2009JB006339

Karlstrom, L., Paterson, S. R., & Jellinek, A. M. (2017). A reverse energy cascade for crustal magma transport. *Nature Geoscience*, *10*(8), 604.

Karlstrom, L., Richardson, P. W., O'Hara, D., & Ebmeier, S. K. (2018). Magmatic landscape construction. *Journal of Geophysical Research: Earth Surface*, *123*(8), 1710–1730.

Kiser, E., Levander, A., Zelt, C., Schmandt, B., & Hansen, S. (2018). Focusing of melt near the top of the Mount St. Helens (USA) magma reservoir and its relationship to major volcanic eruptions. *Geology*, *46*(9), 775–778.

Lees, J. M. (2007). Seismic tomography of magmatic systems. *Journal of Volcanology and Geothermal Research*, *167*(1–4), 37–56. https://doi.org/10.1016/j.jvolgeores.2007.06.008

Lerner, Allan H., 2020, "Supplemental data for “The Prevalence and Significance of Offset Magma Reservoirs at Arc Volcanoes”", https://doi.org/10.7910/DVN/LHD1HY, Harvard Dataverse, V1, UNF:6:5hR78pqI20lJ73cnXYjLYA== [fileUNF]

Lipman, P. W. (1997). Subsidence of ash-flow calderas: relation to caldera size and magma-chamber geometry. *Bulletin of Volcanology*, *59*(3), 198–218.

Lisowski, M., Dzurisin, D., Denlinger, R. P., & Iwatsubo, E. Y. (2008). *Analysis of GPS-measured deformation associated with the 2004-2006 dome-building eruption of Mount St. Helens, Washington: Chapter 15 in A volcano rekindled: the renewed eruption of Mount St. Helens, 2004-2006*. US Geological Survey.

Lu, Z., & Dzurisin, D. (2014). InSAR imaging of Aleutian volcanoes. In *InSAR Imaging of Aleutian Volcanoes* (pp. 87–345). Springer.

Lundgren, P., Samsonov, S. V., López Velez, C. M., & Ordoñez, M. (2015). Deep source model for Nevado del Ruiz Volcano, Colombia, constrained by interferometric synthetic aperture radar observations. *Geophysical Research Letters*, *42*(12), 4816–4823.

Maccaferri, F., Bonafede, M., & Rivalta, E. (2011). A quantitative study of the mechanisms governing dike propagation, dike arrest and sill formation. *Journal of Volcanology and Geothermal Research*, *208*(1–2), 39–50.

Magee, C., Muirhead, J. D., Karvelas, A., Holford, S. P., Jackson, C. A., Bastow, I. D., et al. (2016). Lateral magma flow in mafic sill complexes. *Geosphere*, *12*(3), 809–841.

Massol, H., Jaupart, C., & Pepper, D. W. (2001). Ascent and decompression of viscous vesicular magma in a volcanic conduit. *Journal of Geophysical Research: Solid Earth*, *106*(B8), 16223–16240.

McTigue, D. F. (1987). Elastic stress and deformation near a finite spherical magma body: resolution of the point source paradox. *Journal of Geophysical Research: Solid Earth*, *92*(B12), 12931–12940.

McTigue, D. F., & Segall, P. (1988). Displacements and tilts from dip-slip faults and magma chambers beneath irregular surface topography. *Geophysical Research Letters*, *15*(6), 601–604.

Mogi, K. (1958). Relations between the eruptions of various volcanoes and the deformations of the ground surfaces around them, *36*, 99–134.

Moran, S. C., Freymueller, J. T., LaHusen, R. G., McGee, K. A., Poland, M. P., Power, J. A., et al. (2008). Instrumentation recommendations for volcano monitoring at US volcanoes

under the National Volcano Early Warning System. *U.S. Geological Survey Scientific Investigations Report 5114*.

NASA JPL. (2013). *NASA Shuttle Radar Topography Mission Global 1 arc second [Data set]*. NASA LP DAAC. Retrieved from https://doi.org/10.5067/MEaSUREs/SRTM/SRTMGL1.003

Pinel, V., & Jaupart, C. (2000). The effect of edifice load on magma ascent beneath a volcano. *Philosophical Transactions of the Royal Society of London. Series A: Mathematical, Physical and Engineering Sciences*, *358*(1770), 1515–1532.

Pinel, V., & Jaupart, C. (2003). Magma chamber behavior beneath a volcanic edifice. *Journal of Geophysical Research: Solid Earth*, *108*(B2), 2072. https://doi.org/10.1029/2002JB001751

Pinel, V., & Jaupart, C. (2004). Magma storage and horizontal dyke injection beneath a volcanic edifice. *Earth and Planetary Science Letters*, *221*(1–4), 245–262.

Rivalta, E., Taisne, B., Bunger, A. P., & Katz, R. F. (2015). A review of mechanical models of dike propagation: Schools of thought, results and future directions. *Tectonophysics*, *638*, 1–42.

Roman, A., & Jaupart, C. (2014). The impact of a volcanic edifice on intrusive and eruptive activity. *Earth and Planetary Science Letters*, *408*, 1–8.

Smithsonian Institution. (2013). Volcanoes of the World, v. 4.3.4 [Data set]. Global Volcanism Program.

Sparks, R. S. J., Biggs, J., & Neuberg, J. W. (2012). Monitoring volcanoes. *Science*, *335*(6074), 1310–1311.

Syracuse, E. M., Maceira, M., Zhang, H., & Thurber, C. H. (2015). Seismicity and structure of Akutan and Makushin Volcanoes, Alaska, using joint body and surface wave tomography. *Journal of Geophysical Research: Solid Earth*, *120*(2), 1036–1052.

Taisne, B., & Jaupart, C. (2009). Dike propagation through layered rocks. *Journal of Geophysical Research: Solid Earth*, *114*(B9).

Tamura, J., & Okada, T. (2016). Ambient noise tomography in the Naruko/Onikobe volcanic area, NE Japan: implications for geofluids and seismic activity. *Earth, Planets and Space*, *68*(1), 1.

University of Washington. (1963). Pacific Northwest Seismic Network. International Federation of Digital Seismograph Networks [Data set]. Dataset/Seismic Network. https://doi.org/10.7914/sn/uw

Vandemeulebrouck, J., Sohn, R. A., Rudolph, M. L., Hurwitz, S., Manga, M., Johnston, M. J., et al. (2014). Eruptions at Lone Star geyser, Yellowstone National Park, USA: 2. Constraints on subsurface dynamics. *Journal of Geophysical Research: Solid Earth*, *119*(12), 8688–8707.

Vargas, C. A., Koulakov, I., Jaupart, C., Gladkov, V., Gomez, E., El Khrepy, S., & Al-Arifi, N. (2017). Breathing of the Nevado del Ruiz volcano reservoir, Colombia, inferred from repeated seismic tomography. *Scientific Reports*, *7*, 46094.

Wallace, P. J. (2005). Volatiles in subduction zone magmas: concentrations and fluxes based on melt inclusion and volcanic gas data. *Journal of Volcanology and Geothermal Research*, *140*(1), 217–240.

White, R., & McCausland, W. (2016). Volcano-tectonic earthquakes: A new tool for estimating intrusive volumes and forecasting eruptions. *Journal of Volcanology and Geothermal Research*, *309*, 139–155.

Wicks, C., de La Llera, J. C., Lara, L. E., & Lowenstern, J. (2011). The role of dyking and fault control in the rapid onset of eruption at Chaitén volcano, Chile. *Nature*, *478*(7369), 374–377.

[Geophysical Research Letters]

Supporting Information for

[The Prevalence and Significance of Offset Magma Reservoirs at Arc Volcanoes]

[Allan H. Lerner[1*], Daniel O'Hara[1], Leif Karlstrom[1], Susanna K. Ebmeier[2], Kyle R. Anderson[3], Shaul Hurwitz[3]]

[[1]Department of Earth Sciences, University of Oregon, Oregon 97403, USA. [2]School of Earth & Environment, University of Leeds, Leeds LS2 9JT, UK. [3]U.S. Geological Survey, Moffett Field, California 94035, USA]

Contents of this file

Text S1. Determination of magma reservoir centroids at arc volcanoes

Text S2. Topographic characterization of volcanic edifices

Text S3. Depth datum

Text S4. Auxiliary Data: Volcanic compositions, Crustal stress regimes, Visualization with Google Earth database

Figure S1. Global distribution of arc volcanoes with geophysically inferred magma reservoirs used in this study

Figure S2. Magma reservoir centroid depths and lateral offsets from edifice centroids for volcanoes in different arc stress regimes

Figure S3. Magma reservoir directional locations relative to subduction convergence angle

Figure S4. Edifice volume compared to magma reservoir offset and edifice radius and aspect ratios

Figure S5. Histograms of magma reservoir lateral offset for deformation and tomographic studies

Figure S6. Histogram of edifice mean diameter scaled by reservoir depth.

Figure S7. The lateral distance and depth differences between tomographically and geodetically inferred magma reservoir centroids at the same volcano.

Figure S8. Comparisons of magma reservoir lateral offset from edifice centroids vs recently active vents

Figure S9. Magma reservoir centroid depths and lateral offsets from edifice centroids vs recent vents.

Figure S10. Histograms of magma reservoir offsets from edifice centroids for different confidence levels in reservoir location and link to the edifice.

Figure S11. Magma reservoir offset from edifice centroid relative to reservoir depth and edifice volume or height.

Figure S12. Histogram of magma reservoir offsets for the full dataset and for volcanoes with passive SO2 degassing

Figure S13. Magma reservoir offset from edifice centroids relative to reservoir depth and edifice volume for full dataset vs for volcanoes with passive SO2 degassing

Figure S14. Notched box and whisker plots comparing edifice volumes for volcanoes of different sizes, structural types, and compositions

Figure S15. Notched box and whisker plots comparing magma reservoir lateral offsets from edifice centroids for volcanoes of different sizes, structural types, and compositions

Figure S16. Notched box and whisker plots comparing magma reservoir depths for volcanoes of different sizes, structural types, and compositions

Figure S17. Non-dimensional reservoir offset relative to depth with power law regressions for small and large volcanoes

Figure S18. Comparison of calculated edifice bounds and centroid locations for Mount St. Helens volcano pre- and post-1980 eruption and debris avalanche collapse

Additional Supporting Information
(Files uploaded separately, available at: https://doi.org/10.7910/DVN/LHD1HY**)**

Table S1. List of volcanoes and key edifice morphology and magma reservoir parameters in this study ("Table1_simplified database" sheet)

Table S2. List of volcanoes and full edifice morphology and magma reservoir parameters in this study ("Table2_full database" sheet)

Table S3. Summary statistics of geophysically inferred magma reservoirs at different volcano types, compositions, and edifice sizes ("Table3_summary statistics" sheet).

Data Set S1. A collection of maps (as a PDF) showing edifice bounds and centroids overlain on topographic maps of each volcano in the database.

Data Set S2. Google Earth database of volcanic edifice bounds and geophysically imaged magma reservoirs.

Introduction

Here we provide an extended methods discussion of data sources and analysis, assessment of uncertainty, and supporting figures relevant to discussion in the main text. Additional datasets include Excel data tables, and PDF containing a maps with volcanic edifice bounds and centroid locations, and a Google Earth (.kmz) database volcanic edifice bounds and geophysically imaged magma reservoir locations.

Text S1. Determination of magma reservoir centroids at arc volcanoes

From an extensive literature survey, we compiled 54 different geophysical studies of arc volcanoes fitting the following criteria:

1) Only arc volcanoes (continental and oceanic), in order to reduce tectonic variability. Most studies are from continental arcs, due to data coverage. We do not subdivide our dataset in terms of open or closed system behavior because this metric is poorly defined for most systems and recently observed behavior is likely a transient state over timescales relevant to volcanic lifespans (10s to 100s kyr).

2) Studies published between 2000-2018, to acknowledge rapid increases in geophysical monitoring capabilities. Where multiple studies exist for an individual volcano, we generally include the most recent study of high confidence, which implicitly assumes that subsequent research continues to build upon previous efforts and becomes more refined. However, we acknowledge that volcanic systems can be highly dynamic, and magma reservoirs and deformation sources vary over time, leading to some credible yet different reservoir identifications at the same volcano. Magma reservoirs were inferred by both tomographic and geodetic means at 11 volcanoes, and we include results of both types of studies in the database as separate reservoirs. At 8 volcanoes, authors using a single technique describe multiple distinct magmatic reservoirs at one volcano, and we include multiple reservoirs locations for these systems.

3) Authors explicitly infer a magma body located 2.5 – 15 km depth beneath the surface. The shallow depth threshold is an attempt to filter out hydrothermal and transient sources from our analysis, as volcanic hydrothermal features are dominantly located in the shallowest upper crust (Fournier, 1999), as well as shallow, more ephemeral dikes and sills. This differs from the recent InSAR compilation of volcanic deformation by Ebmeier et al. (2018), which included signals described by shallow geodetic sources attributed to both magmatic and hydrothermal processes. As imaging resolution decreases with increased depth, we impose a lower depth threshold of 15 km to exclude deeper crustal features.

Overall, our compilation includes 47 geodetically inferred magma reservoirs (30 via InSAR, 8 via ground-based GPS, 1 via a leveling survey, 8 via combined geodetic means), and 30 tomographically inferred magma reservoirs (24 via seismic tomography, 4 via MT tomography, 1 via seismic reflection, 1 via seismic receiver functions). Collectively, these studies identified 77 distinct magmatic bodies at 56 volcanic systems, where 18 volcanoes have multiple inferred magma reservoirs (Tables S1, S2, Figure S1). We note that over 100 geophysical studies at 70 additional arc volcanoes were investigated but ultimately excluded from our database for failure to meet our required inclusion criteria.

As discussed in the main text, tomographic and geodetic studies are sensitive to the presence of magma storage regions in different ways and potentially over different timescales.

In contrast to geodetic studies, which require active volume changes in the crust, seismic and MT tomography can identify crustal anomalies related to static magma reservoirs, including those with relatively low melt fractions (although melt fraction is challenging to uniquely constrain). Tomographic studies, however, often have relatively lower spatial resolution compared to geodetic surveys, so that smaller magmatic zones may be recognized preferentially by InSAR or GPS. The substantial disagreement between geodetic and tomographic techniques seen in recognizing magmatic features at single volcanoes (Figure S7) is likely due to co-occurring subsurface magmatic features that express in different ways depending on measurement technique.

Given the wide range of data analysis techniques, model variability, and instrumentation, it is challenging to normalize published studies. Therefore, we have limited our analysis to include only magma reservoirs that are explicitly claimed in refereed publications. We exclude studies that are equivocal in identifying subsurface features as being hydrothermal or fracture zones rather than magmatic bodies. We do not attempt to include any constraints on size of the inferred magma reservoirs as this would require an arbitrary cutoff threshold in what anomaly values defined the "edges" of a magmatic body. Rather, we focus our analysis on the centers of deformation sources and tomographic anomalies to represent magma reservoirs. Where information is provided, we use author-defined latitude, longitude, and depth of the centers of deformation or tomographic features identified by the authors. The hypocenter (latitude, longitude, depth) of magma body centroids are typically defined in geodetic pressure source models, but are rarely explicitly defined in tomographic studies; in these cases, we pick magma body centroids from published figures and descriptions in the text. Seismic features interpreted as magmatic bodies in our database typically have V_p anomalies of -10 to -15%, V_s anomalies of -15 to -30%, and V_p/V_s anomalies of +10 to +30% (Jaxybulatov et al., 2011; Kiser et al., 2018; Tamura & Okada, 2016). Magnetotelluric features interpreted as magmatic bodies typically have resistivity anomalies of 1 - 10 Ωm, which is generally -95 to -99% of the regional background resistivity (Comeau et al., 2015; Hill et al., 2015). Geodetic inflation and deflation sources are usually modeled as inflating spheres in an elastic half space (McTigue, 1987; Mogi, 1958), where lateral position is generally better constrained than source depth or volume change. A number of studies recognize vertically extensive zones suggestive of dike complexes, which makes the definition of a single magma body centroid effectively meaningless, and we exclude such cases from our database.

How accurate are subsurface locations of magma reservoirs?

In this study, we assume published magma reservoir locations have been sufficiently scrutinized and faithfully represented free from confirmation-biases. Compiling such diverse data sources, with each study having varying degrees of reported error analysis and uncertainties, precludes defining a rigorous and consistent uncertainty in inferred magma reservoir locations. We also note a lack of consistency in what reference datum magma body depths are reported in the literature (e.g., relative to sea level, surface elevation, or to the geoid). When unstated in published studies, we attempt to determine the reference datum from text and figures. Most tomographic studies present results using vertical cross sections and horizontal depth slices, which provide very limited views of three-dimensional models. Consequently, defining the true centroids of tomographic anomalies from figures is imprecise. However, the overall uncertainty in our tomographic magma reservoir centroid determinations is usually small compared to their often substantial lateral offset and depth locations. We also consider that errors in our centroid determinations would be non-systematical so that the overall interpretations derived from this database should not be biased. To aid in future

compilations, we suggest that tomographic and geodetic studies publish centroid details (latitude, longitude, depth, and uncertainty) for major anomalies referenced in the text, and also explicitly define the reference datum for depth.

How robust are the links between inferred subsurface magma reservoirs and particular volcanic edifices?

In most cases, magma reservoirs have been associated with the closest most recently active volcanic edifice. However, subsurface features may not necessarily be part of the plumbing system of the nearest recently active edifice – magma reservoirs could be linked to less active volcanic edifices, or may not be related to singular surface volcanic expressions at all, such as in monogenetic fields. The connection between a subsurface magmatic feature and any particular surface landform is robust only if an eruption occurs and a connection can be clearly mapped between magma body and eruption site.

In order to quantify uncertainties associated with reservoir centroid locations, we developed a confidence quality factor based on author interpretations, the quality of data coverage (e.g., number of stations, ray path coverage, duration of measurement or number of InSAR acquisitions, goodness of model fits, and author-stated accuracy and precision), and independent corroborative evidence (e.g., petrologic geobarometry studies or earthquake locations around magma reservoirs). We perform a similar assessment to evaluate the confidence that each magma reservoir is reasonably associated to the nearby volcanic edifice. In this case, we follow the approach of Ebmeier et al. (2018) and highlight the subset of magma reservoirs (n=15) that are linked explicitly to eruptions from their associated edifice (Figures S10, S11). These co-eruptive links are identified either through tracking earthquakes between the magma body and the erupting edifice, or via precursory or syn-eruptive geodetic or tomographic changes (e.g., Nevado del Ruiz, Columbia; Tungurahua, Ecuador; Kirishima, Japan; Asama, Japan; Sakurajima, Japan; Unzen, Japan).

Magma reservoirs with co-eruptive links to the associated edifice are slightly more centrally located than the full dataset (27% vs 34% of reservoirs are laterally offset > 4 km, respectively) (Table S3). However, nine of 13 magma reservoirs with co-eruptive links occur at large volcanoes (volume >43 km^3), which overall have less offset reservoirs (24% of reservoirs at large volcanoes are laterally offset > 4 km). Therefore, reservoirs with co-eruptive links have very similar degrees of offset as the full set of reservoirs at comparably sized volcanoes.

Magma reservoirs with lower confidence in either subsurface locations or in their connectivity to nearby edifices are more laterally offset (10 reservoirs; 80% offset > 4 km) than the full database. The low confidence classification of these studies are partially influenced by the distance of the inferred reservoir from the edifice, which we acknowledge leads to some degree of circular reasoning. However, when excluding the lower quality studies from the database, the overall distribution of magma reservoirs relative to volcanic edifices is not dramatically different from considering the full database (27% vs 34% of reservoirs are laterally offset > 4 km, respectively).

An additional way to assess connectivity between edifices and active magma reservoirs at depth is the occurrence of active magmatic degassing. We incorporate a compilation of volcanoes passively degassing sulfur dioxide (SO_2) recognized by the Ozone Mapping Instrument (OMI) satellite (Carn et al., 2017), in order to identify which volcanoes in our dataset had a clear hydraulic connection to magma at depth. Of the 56 volcanoes in our dataset, 20 volcanoes (hosting 30 inferred magma reservoirs) had OMI-detected passive SO_2 degassing between 2005 - 2015. We note that there are numerous reasons that magma reservoirs at depth may not result in observable SO_2 degassing (magma is too deep or too S-poor to reach volatile saturation,

the reservoir is small so SO_2 emissions are low, SO_2 can by scrubbed by groundwater, OMI satellite resolution may be poor for certain latitudes and altitudes). Still, we observe that SO_2 degassing and non-degassing volcanoes have similar proportions of centralized and offset inferred reservoirs locations (33% of magma reservoirs are laterally offset > 4 km at SO_2 degassing volcanoes) (Figures S12, S13). This recognition, in addition to co-eruptive evidence of some offset reservoirs, lends further support that laterally offset reservoirs may indeed be connected to edifices.

Text S2. Topographic characterization of volcanic edifices

Defining what constitutes a volcanic edifice is not always straightforward, particularly in complex terrain and where numerous volcanic vents are closely located (e.g., volcanic complexes). To map the topography of volcanic edifices, we first define which landforms are likely related to a given volcanic system. We classify volcanoes into four types: stratovolcanoes (25 volcanoes; 34 magma reservoirs), volcanic complexes (16 volcanoes; 22 reservoirs), calderas (including stratovolcanoes with summit calderas) (9 volcanoes; 10 reservoirs), and calderas with ring-fracture vents that formed post-collapse (6 volcanoes; 11 reservoirs) (Tables S1, S2). The classifications for volcanoes in the database are generally taken from the Global Volcanism Project's (GVP) databases of Holocene and Pleistocene volcanism (Smithsonian Institution, 2013). However, for a number of volcanoes, we modified the GVP classifications based on edifice structural and petrologic relationships to other features (e.g., calderas and ring fracture vents, volcanic complexes). As an example, at the Sisters volcanic cluster (Oregon, USA) a number of composite volcanoes are located in close proximity. However petrologic evidence indicates that North, Middle, and South Sister volcanoes tap notably different magmas from presumably different crustal depths (Calvert et al., 2018; Hildreth, 2007), and we thereby classify these as separate edifices (where a geodetically modeled magma body is associated with the nearest edifice, South Sister). Based on such considerations, where information is available, we reclassified certain GVP-defined stratovolcanoes as "volcanic complexes" and *vice versa*. If a summit caldera > 5 km diameter is present, we reclassify stratovolcanoes as "calderas". GVP-defined stratovolcanoes and calderas with clearly related post-caldera vents along ring fractures are reclassified as "caldera ring fracture vents" to avoid considering the post-caldera features as independent edifices.

To make the topographic characterization of volcanic edifices systematic and repeatable, we utilize the Modified Basal Outlining Algorithm (MBOA) (Bohnenstiehl et al., 2012) for defining the outset bounds of features. The MBOA algorithm expands upon the typical closed contour basal analysis method for defining volcanic features, while also accounting for background slope and the presence of other nearby topographic features. We use a global 30 m digital elevation dataset collected in February 2000 from NASA's SRTM-1 global topography mission (NASA JPL, 2013), and include bathymetric datasets from the ETOPO1 mission (Amante & Eakins, 2009) for offshore edifices, where available. Data Set S1 and the Google Earth database (Data Set S2) include figures and shape files showing all quantified edifice boundaries for volcanoes in this database.

Topography within the volcanic edifice basal contour is used to determine the topographic moments via:

$$M_{i,j} = \int \int x^i \, y^j \, Z(x,y) \, dy \, dx, \qquad (1)$$

where *(i,j)* define moment order, *(x,y)* are spatial coordinates in latitude and longitude, and *Z(x,y)* is topography. $M_{0,0}$ is total edifice volume and $M_{1,0}$ and $M_{0,1}$ are the first-order moments in the x and y directions, respectively (Flusser et al., 2016). The center of topography in the x and y directions are calculated as

$$\frac{M_{1,0}}{M_{0,0}} \text{ and } \frac{M_{0,1}}{M_{0,0}}, \quad (2)$$

which together define the edifice centroid.

Mean edifice radius was calculated from the distance between the edifice centroid and edifice bounds measured in 1 azimuthal degree increments. We note that our calculated edifice volumes are generally conservative and may not necessarily reflect total eruptive volumes, given distal outfall volumes and the effects of erosion, collapses, and other non-volcanic processes on volcano edifices (e.g., South Sister edifice calculated at 11 km^3 and MSH at 43 km^3 compared to estimates by Hildreth [2007] of 20 km^3 and 40-50 km^3 for total erupted volume for each respective volcano, which includes distal fallout deposits). Additionally, we do not attempt to account for past erosion and flank collapses that may affect our edifice centroid and volume calculations. However, in comparing the recent example of topographic changes at Mount St. Helens from before and after the 1980 eruption, where the debris avalanche and eruption removed ~2.5 km^3 of material from the summit and north flank, we observe only a very minor shift in edifice centroid position of 190 m to the SSW (Figure S18). Although the 1980 events caused dramatic changes to the volcano topography, our calculations of edifice volume and centroid are largely determined by the broad basal distribution of volume, so that the remobilized volume at Mount St. Helens was a small component of the overall volcano size. Extending this observation more generally, edifice volume and centroid location are unlikely to change drastically over short timescales, barring very major caldera collapses or flank collapses that remove huge portions of the edifice. In summary, our approach provides a reproducible, globally applicable, and objective means to characterize edifice sizes and centroid positions.

Edifice topographies for 9 volcanoes with 13 inferred magma reservoirs were undefined due to highly complex topography or because of low-lying or negative volcanic landforms. These volcanic systems are typically subaqueous or partially submerged calderas where sufficiently resolved bathymetry is unavailable (e.g., Rabaul Caldera, Papua New Guinea), broad volcanic fields lacking prominent topography (e.g., Laguna del Maule, Chile), or in complex terrain where edifices cannot be easily isolated from non-volcanic structures (e.g., Santorini, Greece; Spurr, USA). In these cases, a rough mean radius was determined by fitting an ellipse to the planform view of the volcano, and the ellipse center was approximated as the edifice center. Edifice volumes and relief were unquantifiable for these volcanoes, and thus are excluded from analyses involving these topographic parameters.

Importantly, we note that by focusing on edifice centroids, we define our volcanic edifice locations differently than volcano locations given in the GVP database, which focuses on locations of recent eruptive vents or volcano summits (which are important for hazard assessment, but are a geologically transient features). Comparing the locations of edifice centroids to the location of the most recently active vents (which we define via historical observations, visible evidence of eruption such as vent craters, or otherwise taken to be the volcano summit), we observe that although edifice centroids and vents are generally roughly co-located, in many cases edifice centroids are multiple kilometers from vent locations. The differences between recent vent locations and edifice centroids are greatest for volcanic complexes and calderas with ring fracture vents (Figure S8). Differences between vent and edifice centroid locations translate into appreciable differences in magma reservoir offset distances from recent vents or from edifice centroids (Figure S9).

Text S3. Depth datum

The lithostatic pressure affecting a subsurface magma body is a function of the overlying crustal rock column averaged over a surface area roughly equal to the reservoir depth (McTigue & Segall, 1988). Given this, and because depths are inconsistently reported in published studies, we recalculate magma reservoir centroids as depth from the mean local surface elevation. The average local surface elevation for each magma reservoir is determined from a circular area around the reservoir centroid epicenter, where the circle's diameter is equal to the depth of the reservoir centroid beneath the surface (Tables S1, S2). Thus, the mean surface elevation is calculated over a smaller surface region for shallower reservoirs than for deeper reservoirs. Given that a substantial number of reservoir centroids are significantly offset from volcano summits, these recalculated depths can be notably different from the more conventional view of assuming depth beneath a volcanic summit. For 6 cases where magma reservoir centroids are subaqueous, we use depth beneath the sea floor as the diameter to average local bathymetry elevation. We then add the 1/3 of the mean water column height to the reservoir depth to account for the pressure that the water column exerts (where water density is ~1/3 that of non-porous crustal rock).

Text S4. Auxiliary Data: Volcanic compositions, Crustal stress regimes, Visualization with Google Earth database

Volcanic compositions: Many volcanic systems exhibit compositional diversity in erupted products in time and space. However, given the scope of our analyses, we consolidate this complexity and classify volcano types as simply "basaltic", "andesitic", "dacitic", or "rhyolitic" based on their dominant rock type, either reported in the GVP database or in recent publications (Tables S1, S2). For bimodal systems, we consider the volcano composition as that of most recent eruption, hereby assuming that inferred magma reservoirs are likely related to the recent activity. Our "basaltic" classification includes GVP dominant compositions of "Basalt/Picro-basalt" and "Trachybasalt/Tephrite Basanite". Our "andesitic" classification includes GVP dominant compositions of "Andesite/Basaltic", "Andesite/Basaltic andesite", and "Phono-tephrite/Tephri-phonolite". Our "dacitic" and "rhyolitic" classifications include GVP dominant compositions of "Dacite" and "Rhyolite", respectively.

Crustal stress regimes: Characteristics of arc stress regime for each volcanic center are from the compilation of Heuret and Lallemand (2005) where stress state is classified on a -3 to +3 scale from highly compressional to highly extensional (Tables S1, S2, Figures S1, S2). This compilation specifically calculates stress state in the back-arc, however these stress states should generally apply to the main volcanic arc as well. The Heuret and Lallemand (2005) compilation does not include arcs in the Mediterranean, so Italian and Hellenic arc volcanoes are excluded from this metric. Some stress regimes are under-represented in our database, so relationships of magma reservoir depth distributions in different stress regimes remain inconclusively resolved.

Visualization with Google Earth database: Volcanic edifice bounds and the locations of edifice centroids, vents, summits, and magma reservoir centroids (with depth information in metadata) have been compiled into a Google Earth database. Image overlays from key publication figures are also included, which were in some cases used to determine the reservoir centroid, or in other cases simply as illustrative examples. This Google Earth database is available as Data Set S2.

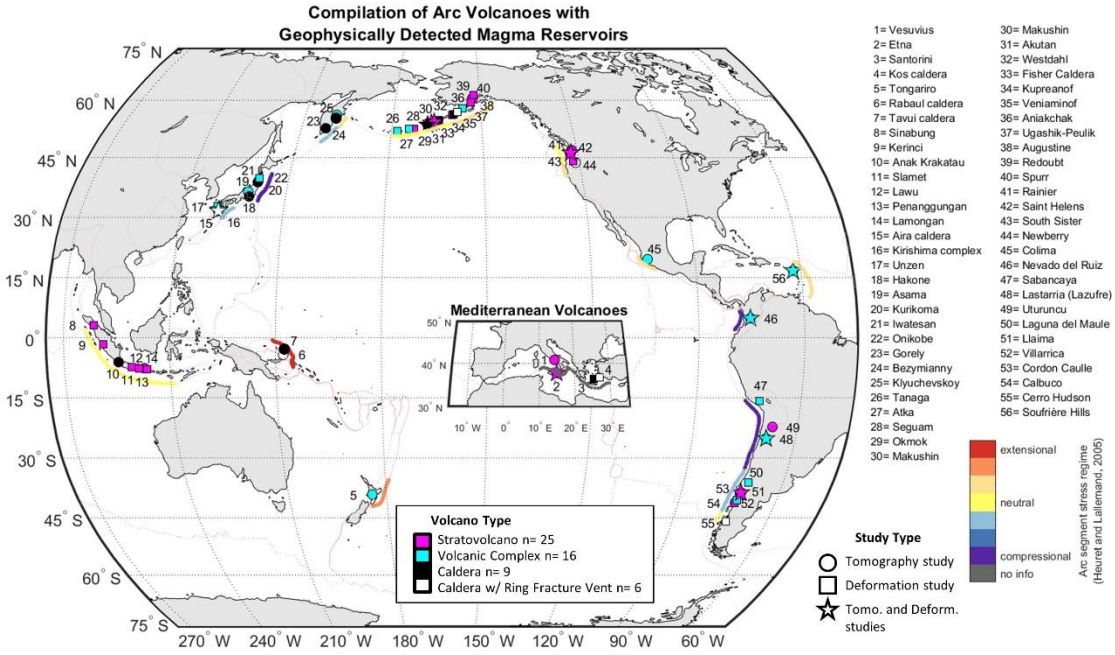

Figure S1. Global distribution of arc volcanoes with geophysically inferred magma reservoirs used in this study. Symbol colors indicate volcanic edifice type and symbol shape indicates the types of geophysical study at each volcano. Subduction zone segments are colored according to back-arc stress regime. Volcanoes are identified by numbers 1 - 56 (see Tables S1, S2).

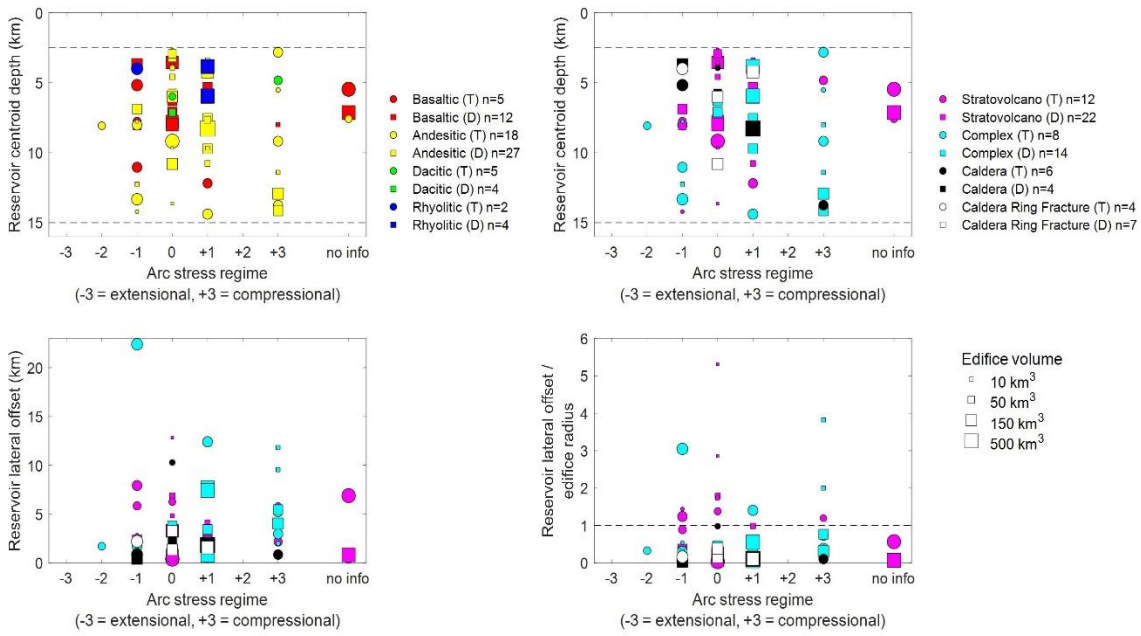

Figure S2. *(top)* Magma reservoir centroid depths and *(bottom)* absolute and scaled lateral offsets from edifice centroids for volcanoes in different arc stress regimes. Arc stress regimes are taken from back-arc stresses defined by Heuret and Lallemand (2005). No stress state was defined for Mediterranean subduction zones, and are listed here as "no info". Symbols sizes are scaled to edifice volumes. *(T)* and *(D)* indicate tomography and deformation studies, respectively. 13 magma reservoirs at volcanoes with unquantified volumes are not shown. Dashed horizontal lines are the shallowest and deepest depths considered in this study.

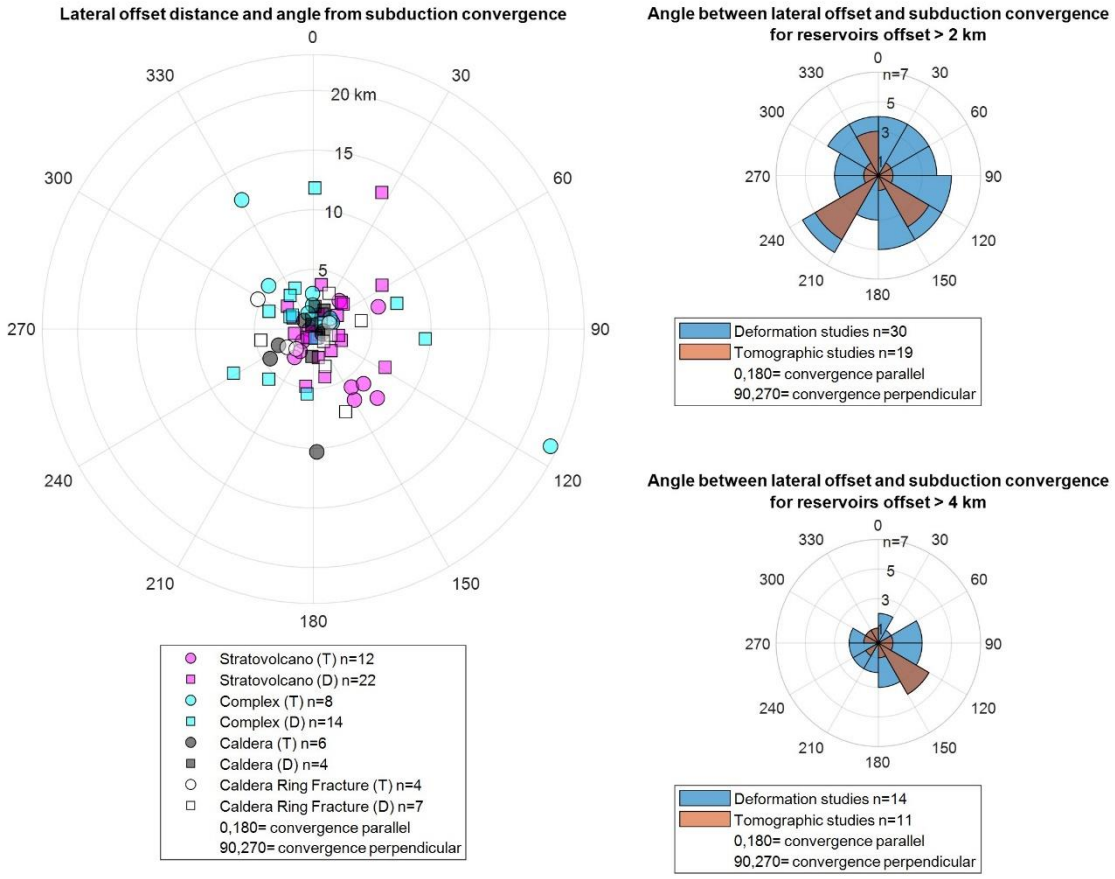

Figure S3. (*left)* Planform view of the lateral offset distance between edifice and magma reservoir centroids, and angle between edifice-reservoir offset direction and the direction of local subducting plate convergence. Directions of 0° and 180° indicate that reservoirs are offset parallel to local subduction plate convergence direction, in directions distal (0°) and proximal (180°) to the trench. Directions of 90° and 270° indicated reservoirs offset perpendicular to plate convergence, along strike of the subduction. (*right*) Polar histograms of magma reservoir offset from edifice centroid relative to convergence direction for reservoirs offset > 2 km *(top)* and > 4 km *(bottom)* from the edifice centroid. Histogram counts are cumulative (not overlapping). Direction of plate convergence in the vicinity of each volcano location is taken from the NNR-MORVEL no net rotation model (Argus et al., 2011).

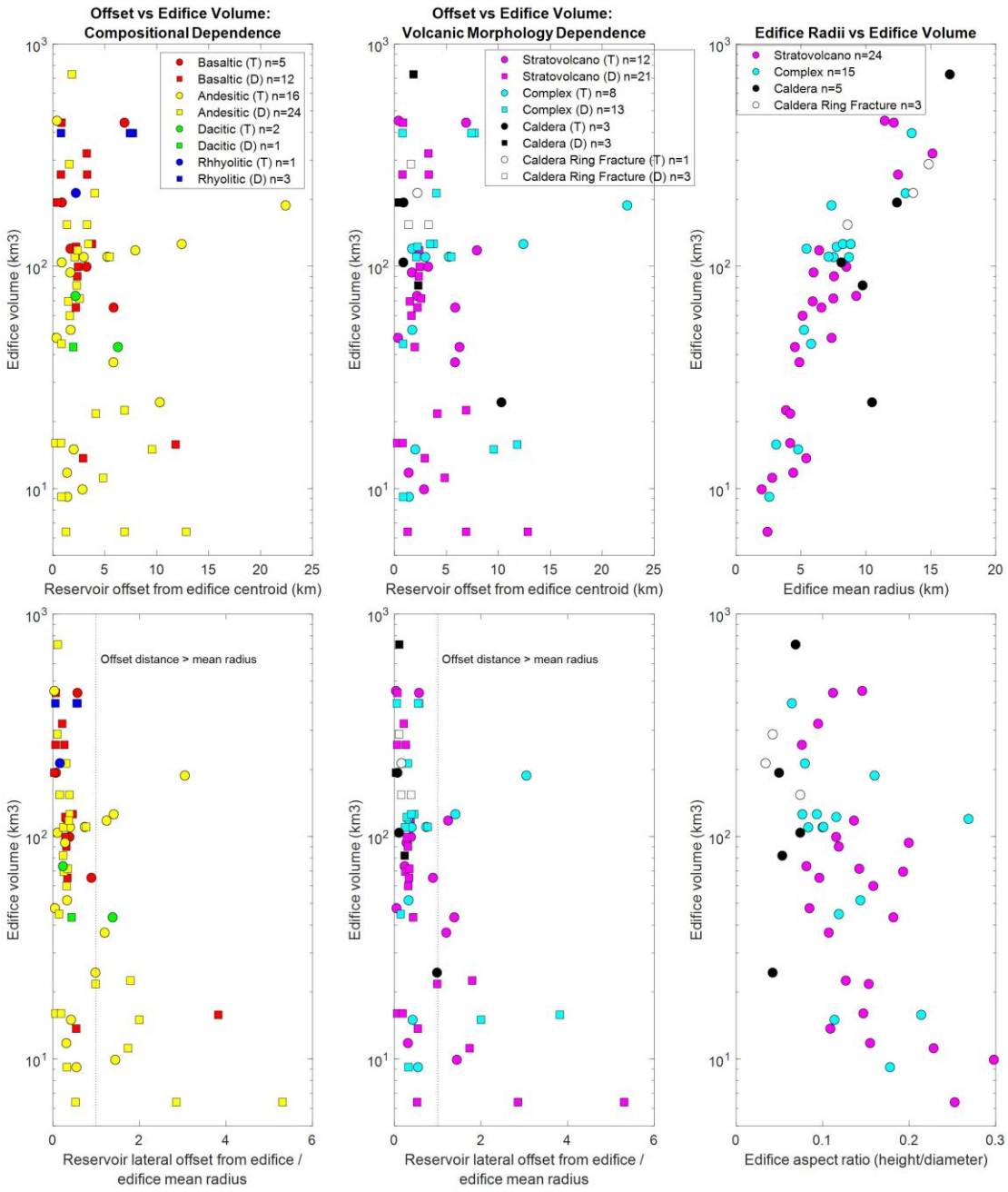

Figure S4. Edifice volume compared to magma reservoir lateral offset and edifice radius and aspect ratios, in absolute *(top)* and scaled *(bottom)* offsets. *(T)* and *(D)* indicate tomography and deformation studies, respectively. 13 magma reservoirs at volcanoes with unquantified volumes are not shown. Legend is the same for sets of upper and lower panels.

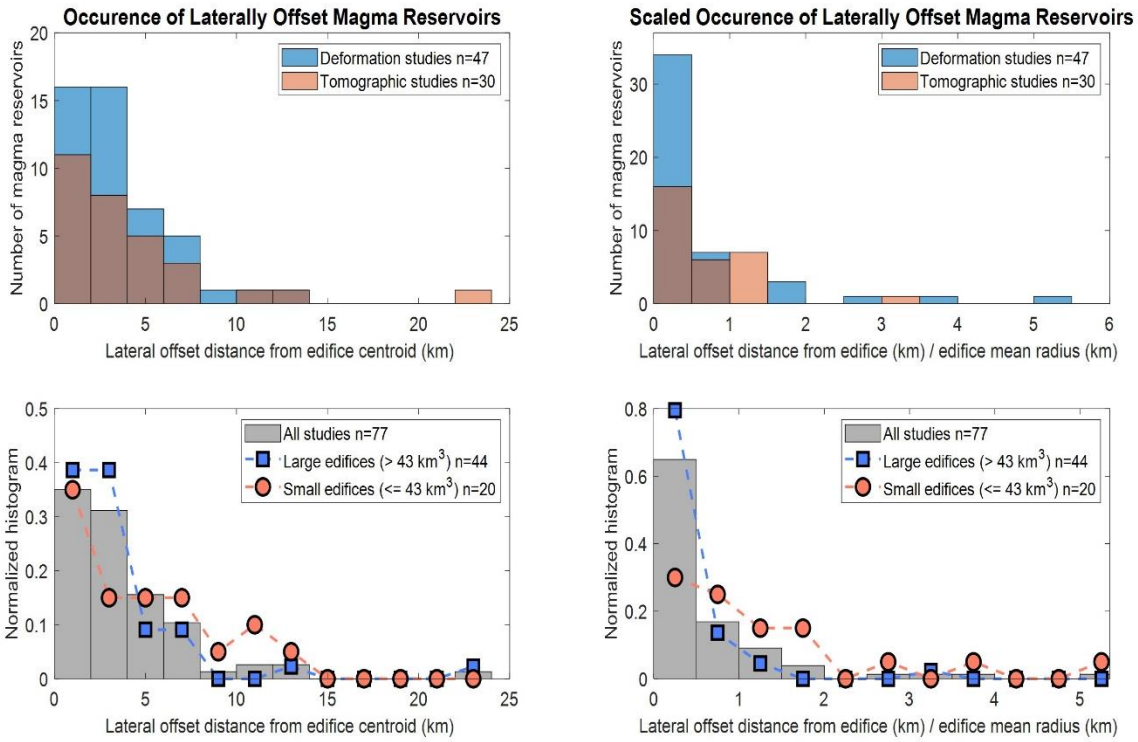

Figure S5. *Upper panels:* Histograms of absolute lateral offset *(top left)* and scaled offset *(top right)* for deformation and tomographic studies. A greater number of geodetically inferred magma reservoirs are included in our database than tomographically located reservoirs, but a similar proportion of reservoirs offset > 4 km are recognized by both techniques (32% vs. 37%, respectively). Histogram counts are overlapping (not cumulative). *Lower panels:* Deformation and tomography studies are combined and the full dataset is separated into large and small edifice volumes for magma reservoir absolute offsets *(bottom left)* and scaled offsets *(bottom right)*. Setting a threshold volume of ≤ 43 km^3, smaller edifices are notably more offset than larger edifices ($p = 0.25$; Figure S15). 13 magma reservoirs at volcanoes with unquantified volumes are not shown in lower panel.

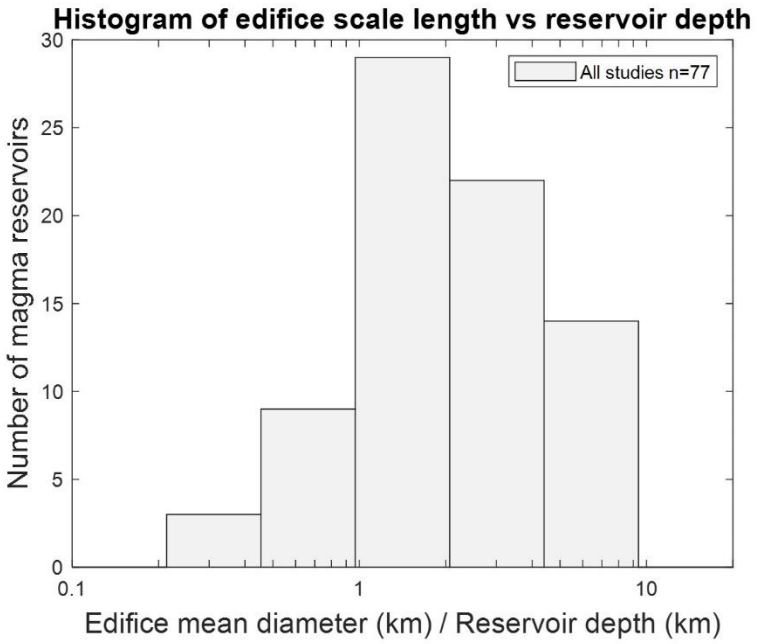

Figure S6. Histogram of edifice mean diameter scaled by reservoir depth. All magma reservoir depths are within an order of magnitude of associated edifice diameters, implying that stresses and deformation from each structure are in phase (McTigue & Segall, 1988) and that sub-volcanic magma reservoirs and their edifices are likely mechanically coupled.

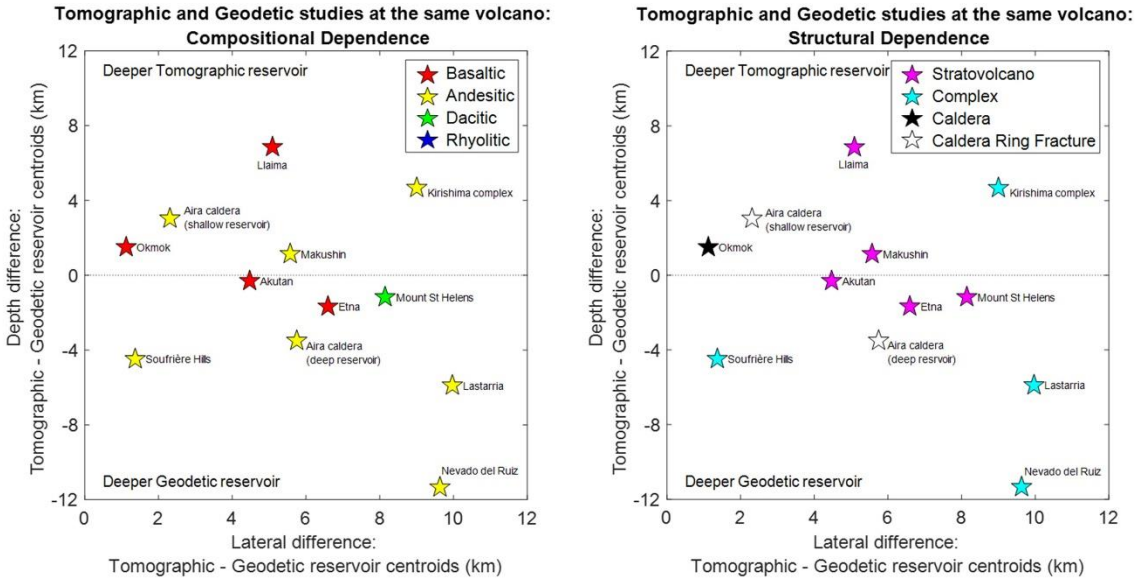

Figure S7. The lateral distance and depth differences between tomographically and geodetically inferred magma reservoir centroids at the same volcano. Volcanoes are categorized by *(left)* dominant composition and *(right)* structural type. Major differences in both depth and lateral position of inferred magma reservoirs exist between the different techniques.

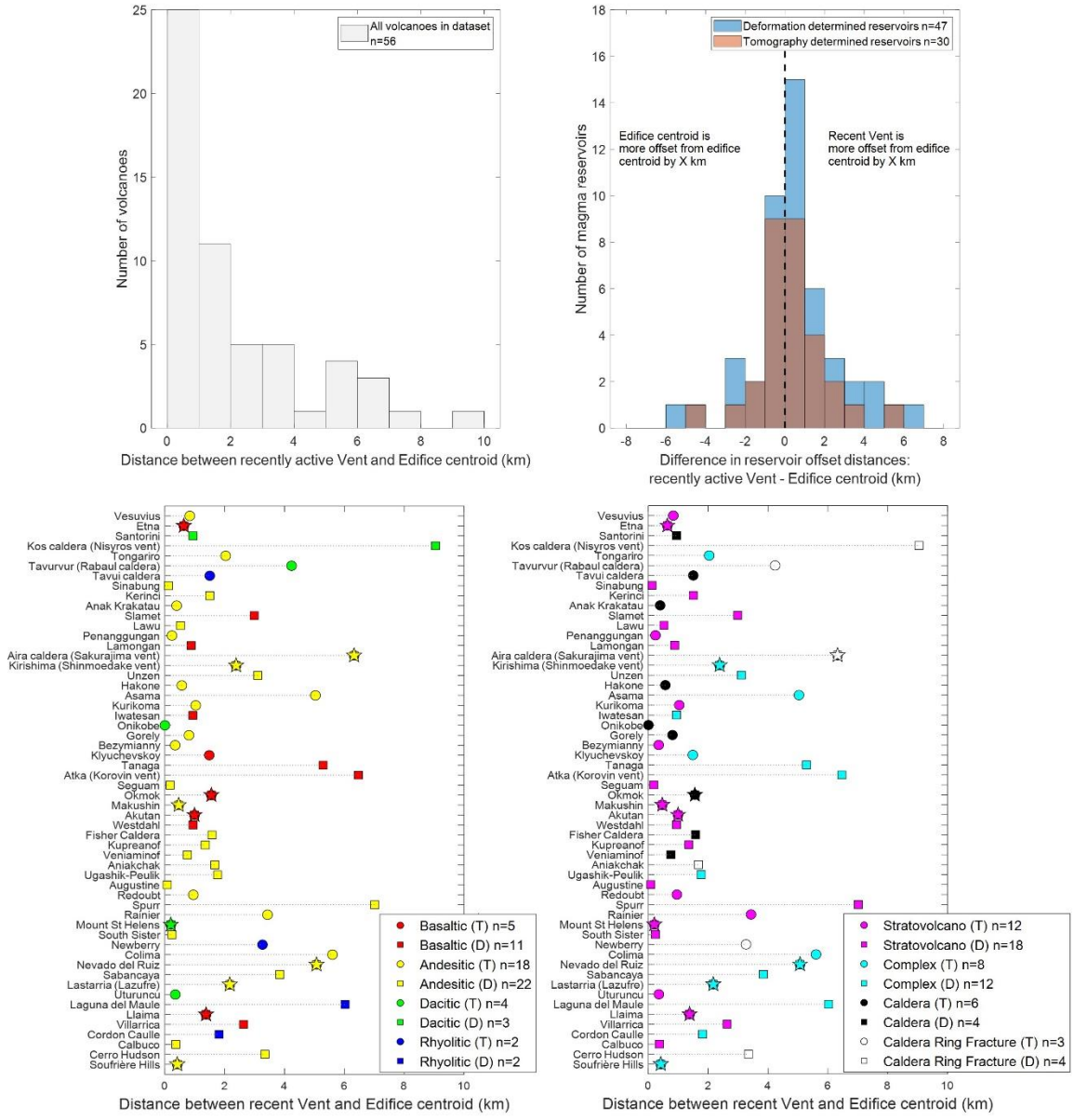

Figure S8. *(top left)* Comparison of edifice centroids and recently active vents (or summits where no vent was identified). Edifice centroids can be substantially removed from vent/summit locations, leading to notable differences in offset distances of magma reservoirs if considering distance from magma reservoir to edifice centroid or to vent location *(top right)*. Histogram counts are overlapping (not cumulative). *(bottom panels)* Distances between edifice centroids and recent vent or volcanic summits for each volcano in this database, with volcanoes classified by composition *(bottom left)* or structural type *(bottom right)*. *(T)* and *(D)* indicate tomography and deformation studies, respectively. Star symbols are volcanoes with magma reservoirs inferred from both tomography and deformation studies.

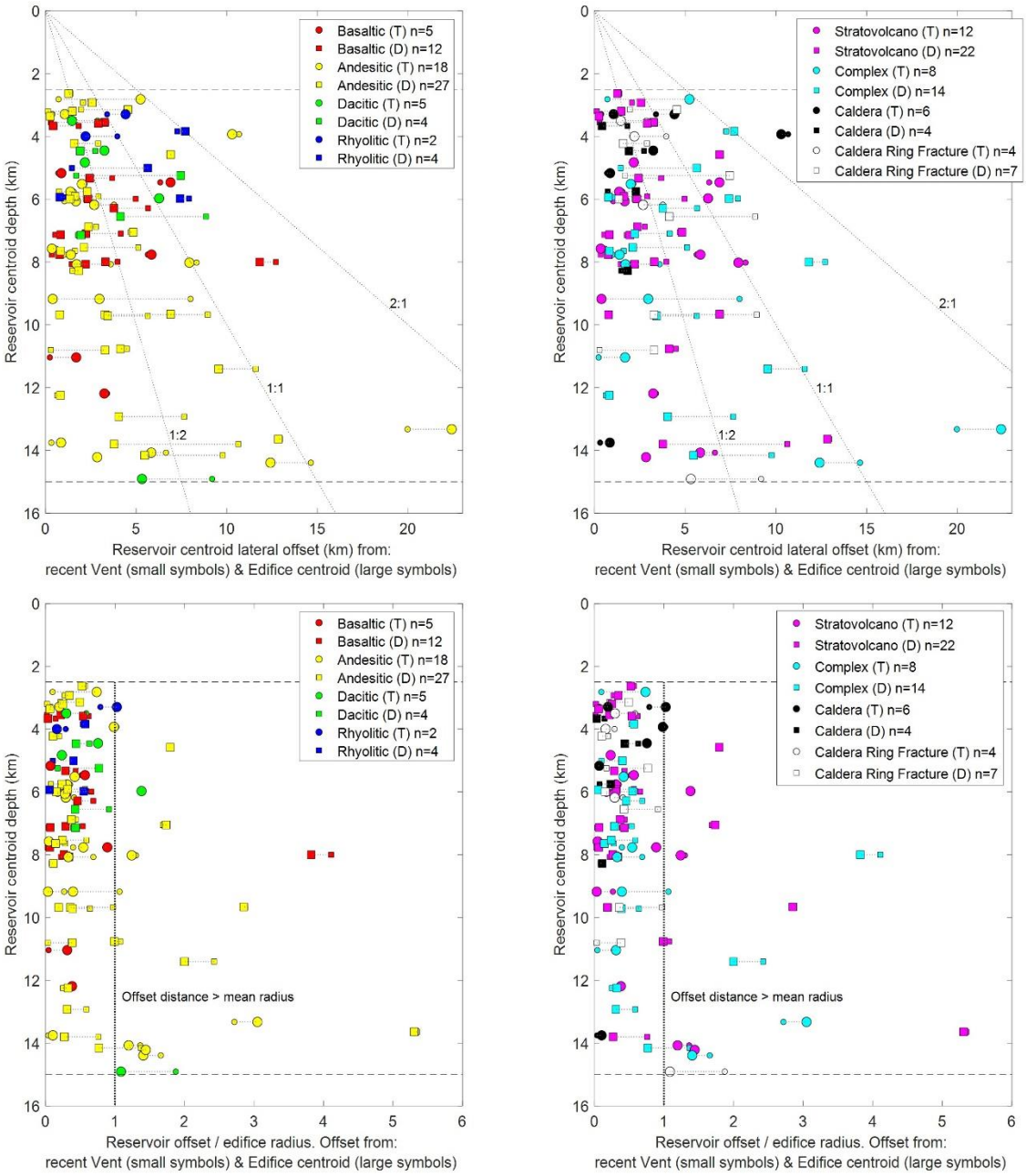

Figure S9. Magma reservoir centroid depths and absolute lateral offsets *(top)* and scaled lateral offsets *(bottom)* from edifice centroids (large symbols) and recent vents (small symbols). Volcanoes are classified by composition *(left)* or structural type *(right)*. *(T)* and *(D)* indicate tomography and deformation studies, respectively. Dashed horizontal lines are the shallowest and deepest depths considered in this study.

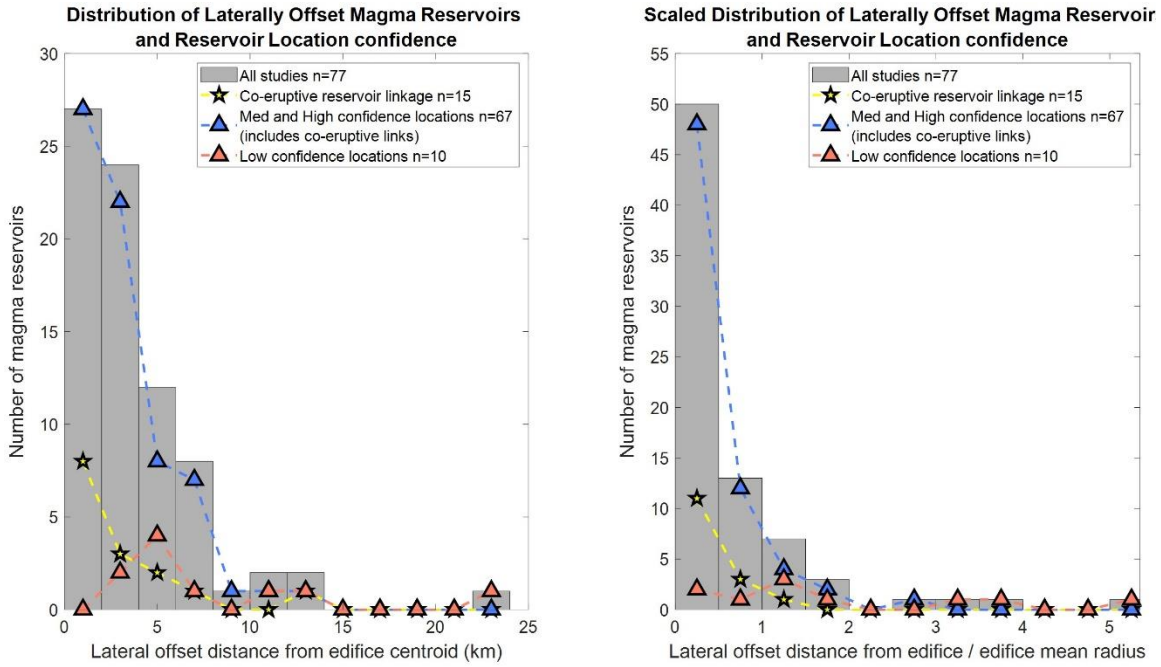

Figure S10. Histograms of absolute *(left)* and scaled *(right)* magma reservoir offsets from edifice centroids for different confidence levels in reservoir location and link to the edifice. Co-eruptive links are identified either through tracking earthquakes between the magma body and the erupting edifice, or via precursory or syn-eruptive geodetic or tomographic changes.

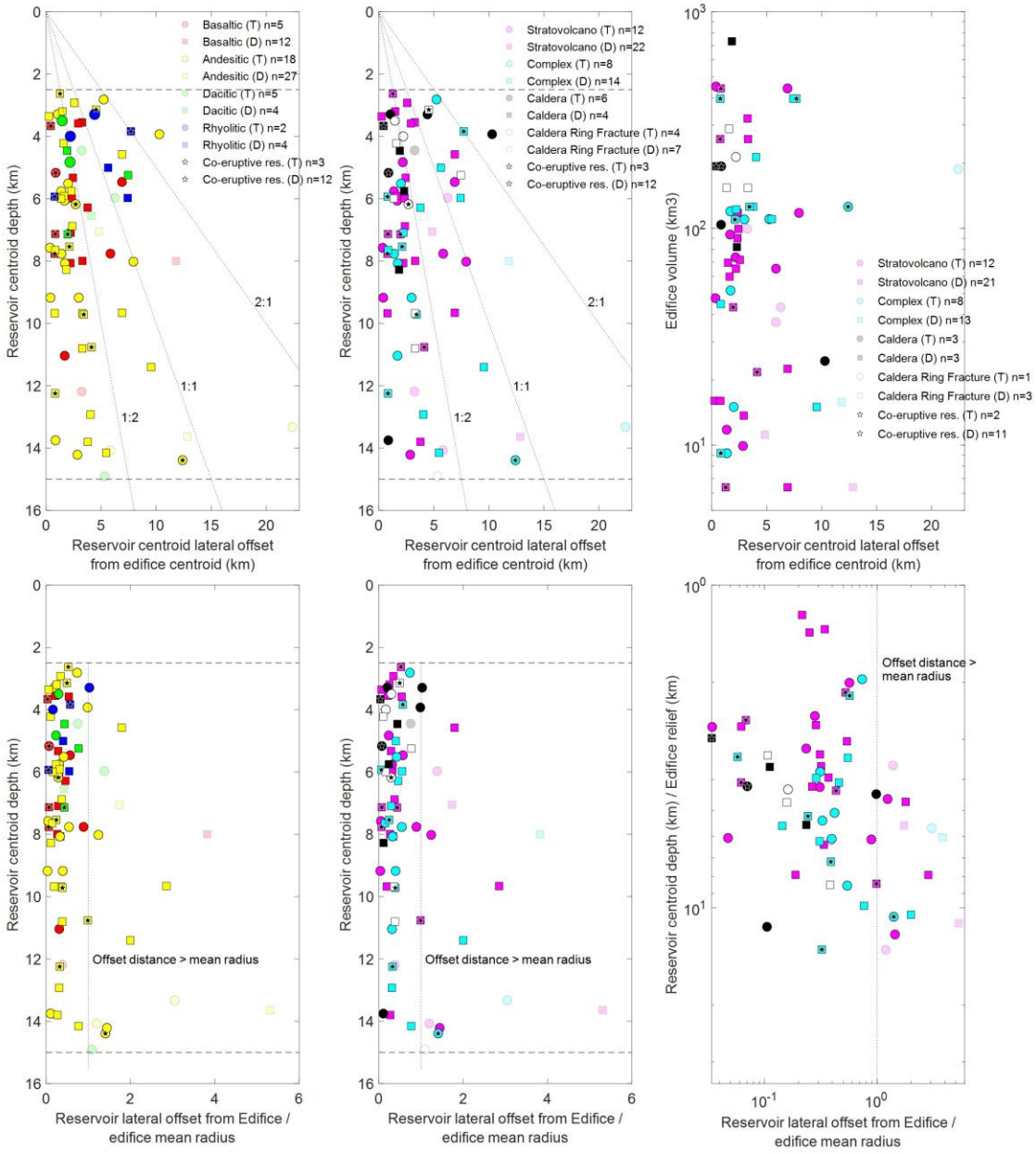

Figure S11. Absolute *(top panels)* and scaled *(lower panels)* magma reservoir centroid offset from edifice centroid relative to reservoir depth and edifice volume or height. Magma reservoir locations with low imaging quality or low confidence in connection to the edifice are shown in transparency (n=10). A subset of magma reservoirs with co-eruptive evidence of occurrence and linkage to the edifice are highlighted with central stars (n=15). Symbols in all left and middle figures are not scaled by edifice volume, so that the 13 reservoirs at volcanoes with unquantified edifice volumes are included in this figure, as opposed to Figures 2 and 3 in the main text. Dashed horizontal lines are the shallowest and deepest depths considered in this study. *(T)* and *(D)* indicate tomography and deformation studies, respectively. Legend is the same for sets of upper and lower panels.

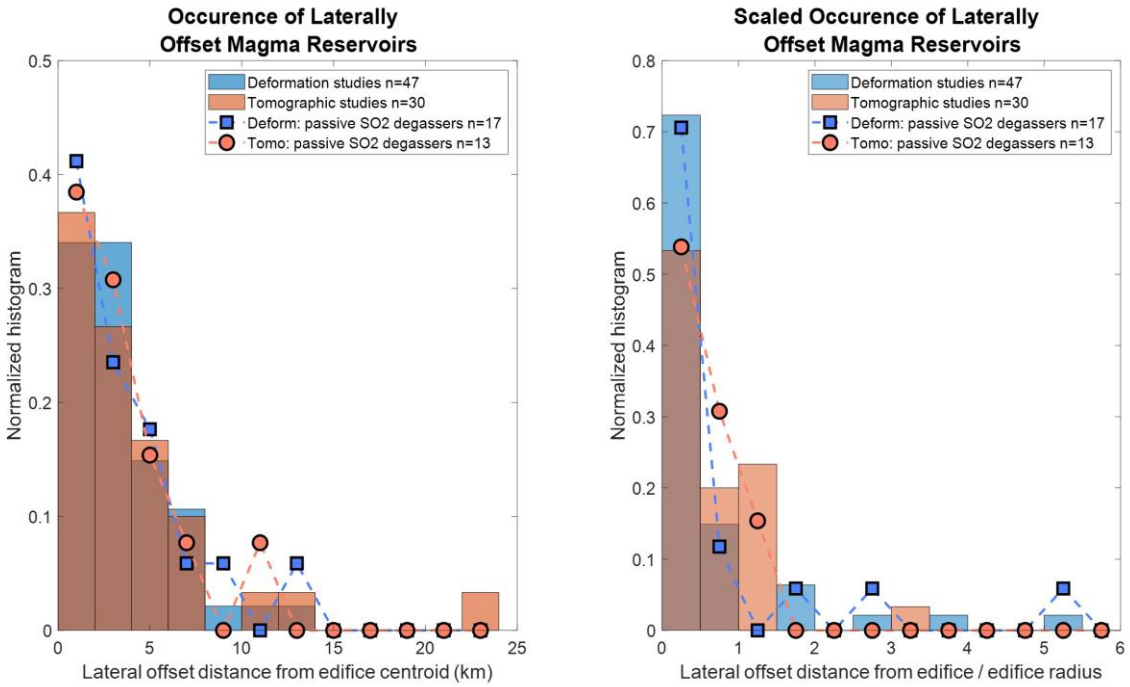

Figure S12. Histogram of magma reservoir absolute offset from edifice centroid *(left)* and offset scaled to edifice radius *(right)* for the full dataset (bars) and for volcanoes with passive SO_2 degassing (lines; 20 volcanoes hosting 30 magma reservoirs) detected between 2005 - 2015 via OMI satellite (Carn et al., 2017). The distribution of reservoir lateral offsets is very similar between volcanoes with passive SO_2 degassing compared to the full database. Histogram bar counts are overlapping (not cumulative).

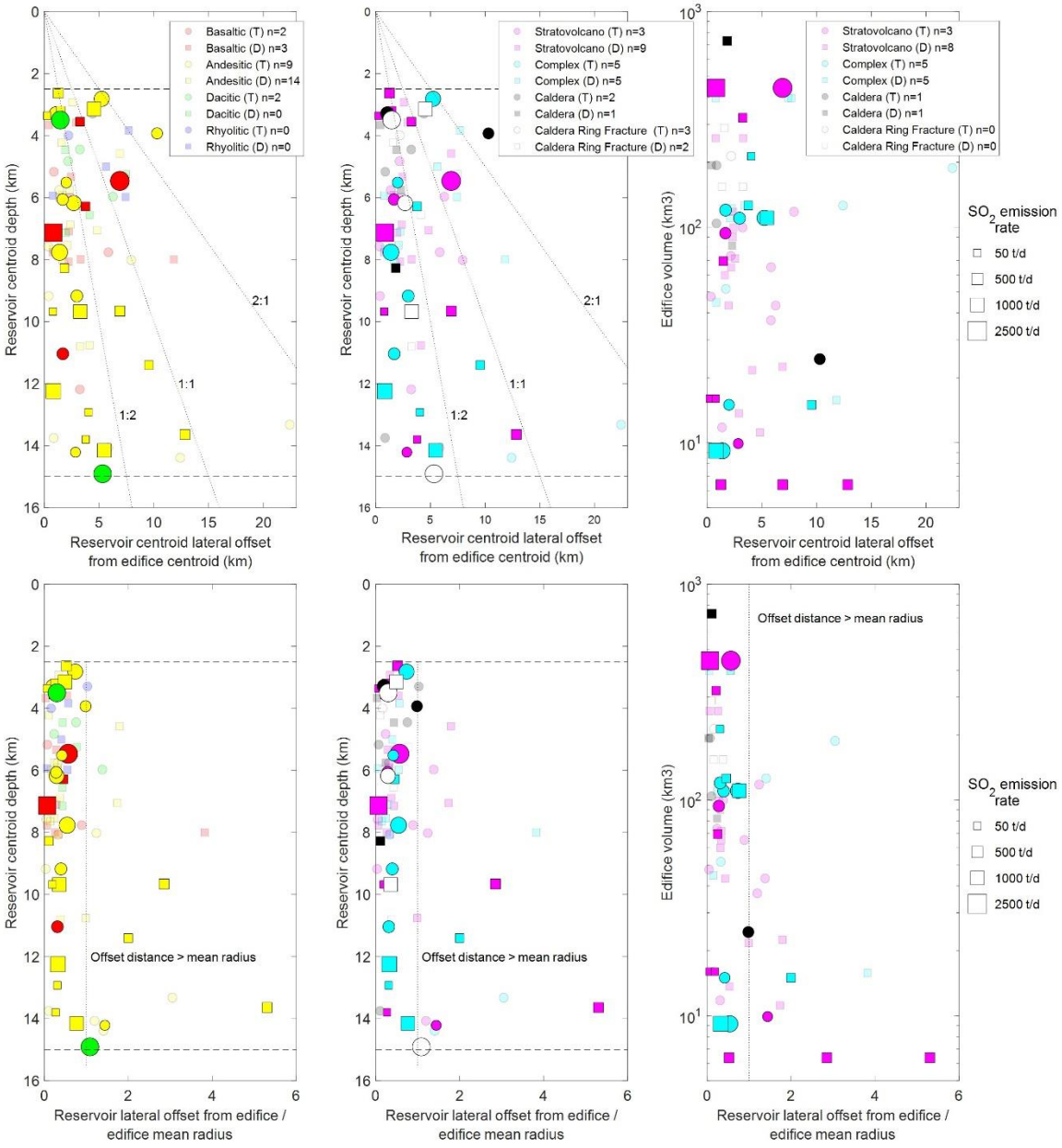

Figure S13. Absolute *(upper panels)* and scaled *(lower panels)* magma reservoir centroid offset from edifice centroid relative to reservoir depth and edifice volume. Volcanoes with passive SO_2 degassing detected between 2005 - 2015 via OMI satellite (Carn et al., 2017) are highlighted (20 volcanoes hosting 30 magma reservoirs), with symbol sizes scaled to average SO_2 degassing rate during the detection time interval. Volcanoes without detected passive SO_2 degassing are shown in transparency (36 volcanoes hosting 47 magma reservoirs). *(T)* and *(D)* indicate tomography and deformation studies, respectively. Legend is the same for sets of upper and lower panels.

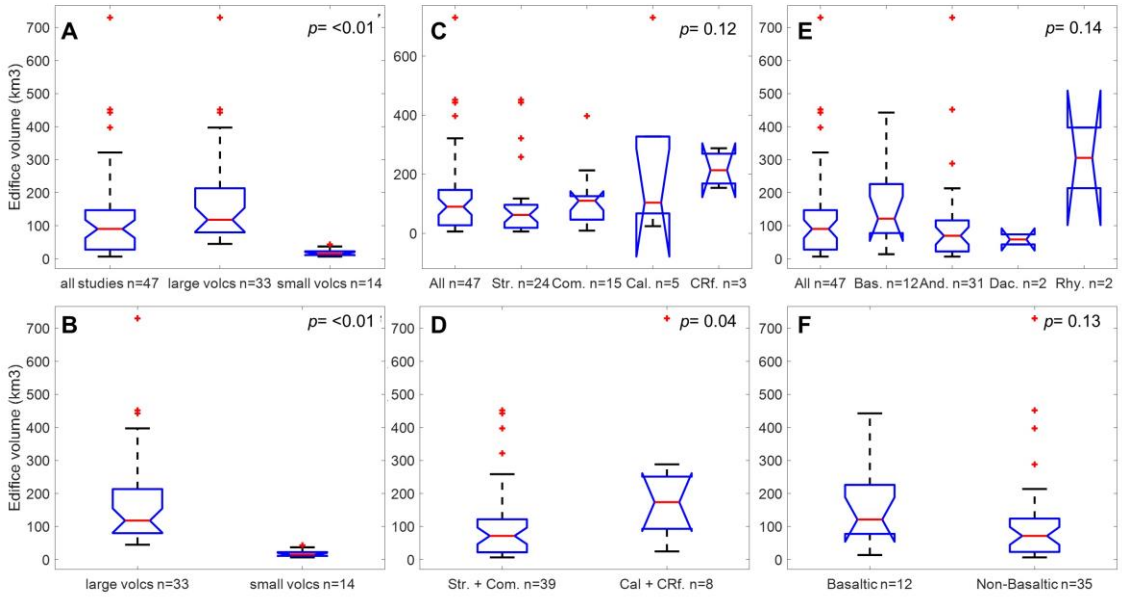

Figure S14. Notched box and whisker plots comparing edifice volumes for volcanoes of different size classifications *(A, B)*, structural types *(C, D)*, and compositions *(E, F)*. The red horizontal line is the median value and the notched area defines the 95% confidence range for the median. *P*-values from Kruskal-Wallis ANOVA tests (non-parametric data) show the probability that all groups are from a single distribution. Volcanoes with edifice volumes ≤ 43 km^3 are considered "small". Str. = stratovolcano; Com. = volcanic complex; Cal. = calderas; CRf. = calderas with ring fracture vents; Bas = basaltic; And = andesitic; Dac = dacitic; Rhy = rhyolitic.

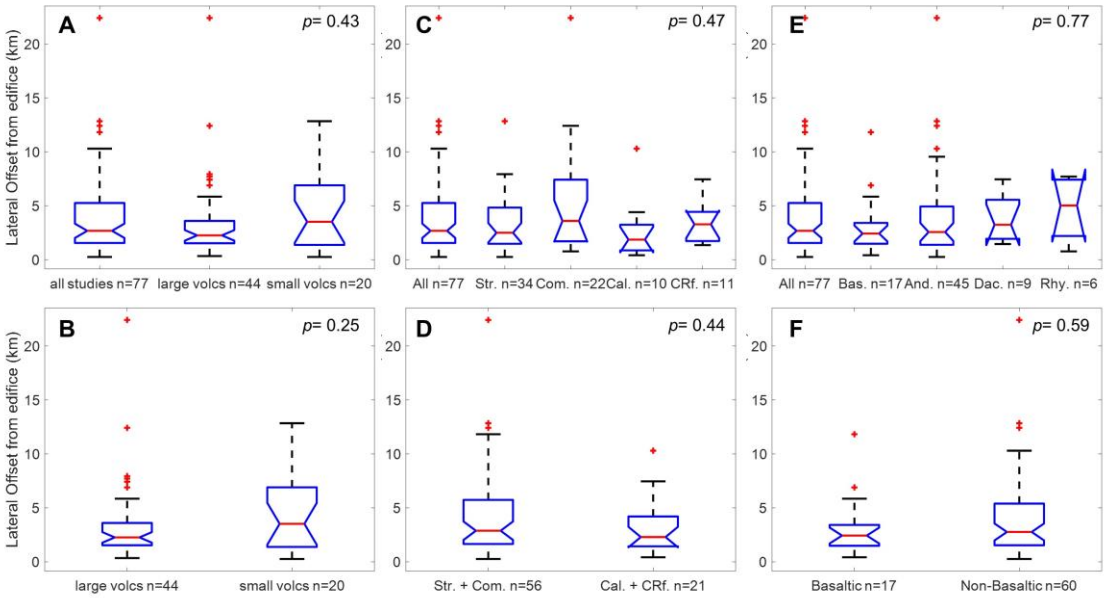

Figure S15. Notched box and whisker plots comparing magma reservoir lateral offsets from edifice centroids for volcanoes of different size classifications *(A, B)*, structural types *(C, D)*, and compositions *(E, F)*. The red horizontal line is the median value and the notched area defines the 95% confidence range for the median. *P*-values from Kruskal-Wallis ANOVA tests (non-parametric data) show the probability that all groups are from a single distribution. Volcanoes with edifice volumes ≤ 43 km^3 are considered "small". Str. = stratovolcano; Com. = volcanic complex; Cal. = calderas; CRf. = calderas with ring fracture vents; Bas = basaltic; And = andesitic; Dac = dacitic; Rhy = rhyolitic.

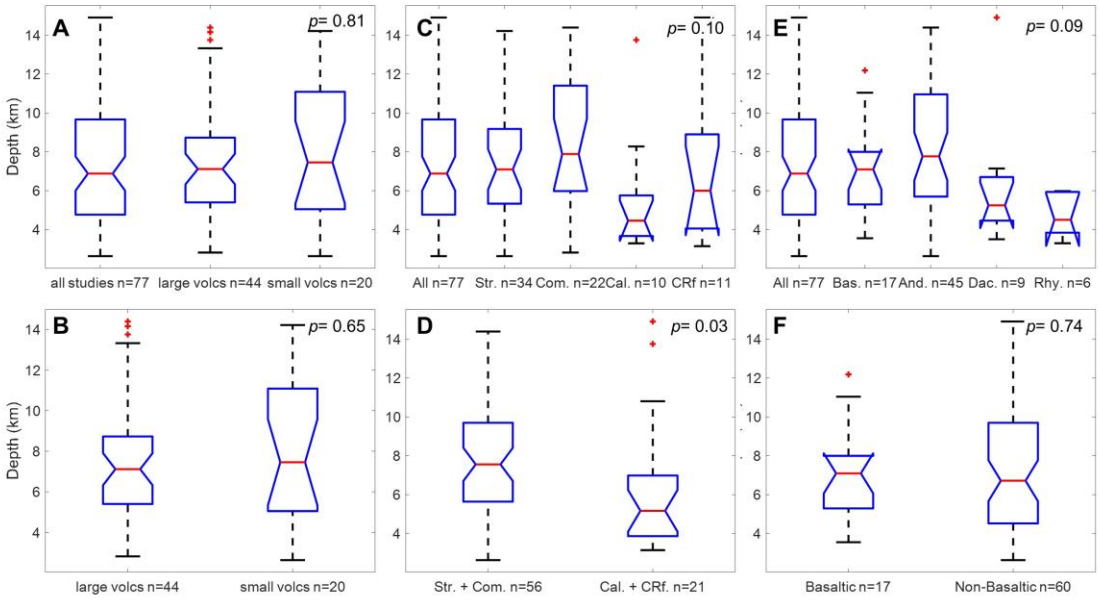

Figure S16. Notched box and whisker plots comparing magma reservoir depths for volcanoes of different size classifications *(A, B)*, structural types *(C, D)*, and compositions *(E, F)*. The red horizontal line is the median value and the notched area defines the 95% confidence range for the median. *P*-values from Kruskal-Wallis ANOVA tests (non-parametric data) show the probability that all groups are from a single distribution. Volcanoes with edifice volumes ≤ 43 km^3 are considered "small". Str. = stratovolcano; Com. = volcanic complex; Cal. = calderas; CRf. = calderas with ring fracture vents; Bas = basaltic; And = andesitic; Dac = dacitic; Rhy = rhyolitic.

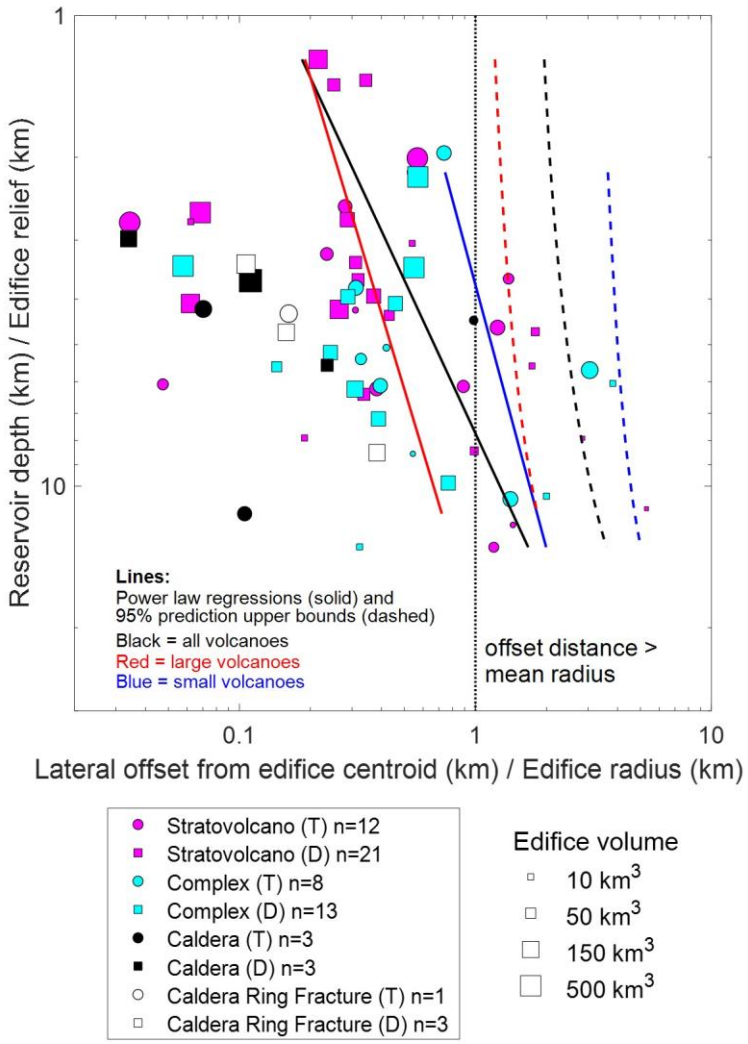

Figure S17. Non-dimensional view of reservoir offset relative to depth (same as Figure 3b in main text). Power law regressions and 80% upper prediction bounds are shown for the full database (black), large volcanoes (red), and small volcanoes (blue). Volcanoes with edifice volumes ≤ 43 km^3 are considered "small". The scaled reservoir lateral offset (x-axis) is taken as the dependent variable. Power laws fits are of the form: $x = b \cdot y^m$, where x is the magma reservoir scaled lateral offset and y is the scaled reservoir depth. Fit coefficients are: All volcanoes: $x = 0.1510 * y^{0.9249}$, $R^2 = 0.15$; Large volcanoes: $x = 0.1667 * y^{0.6006}$, $R^2 = 0.05$; Small volcanoes: $x = 0.4925 * y^{0.5374}$, $R^2 = 0.10$. *(T)* and *(D)* indicate tomography and deformation studies, respectively. 13 magma reservoirs at volcanoes with unquantified volumes are not included in the figure or in regression fitting.

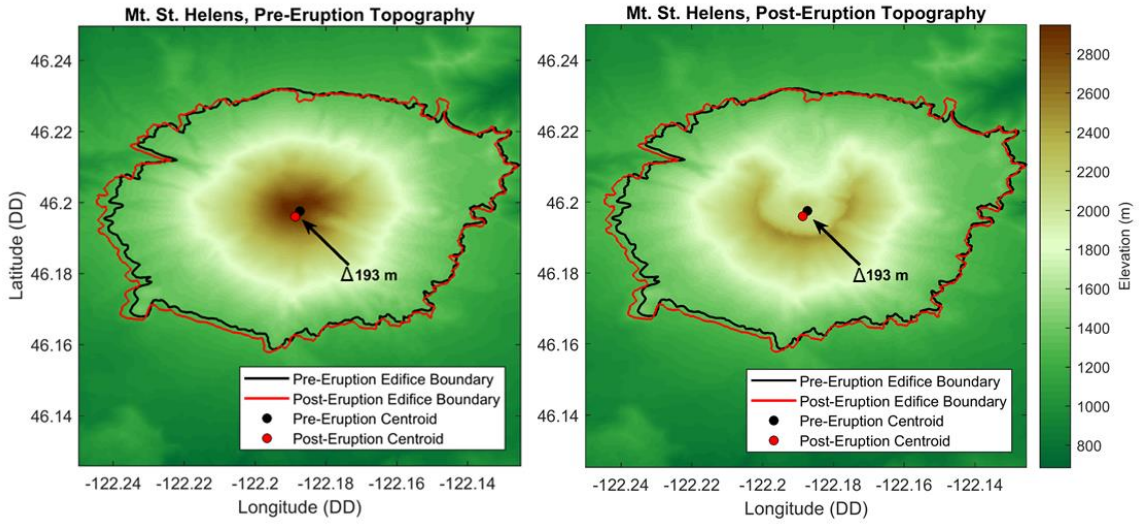

Figure S18. Surface topography of Mount St. Helens volcano (WA, USA) *(left)* before and *(right)* after the 1980 eruption and flank collapse/lateral blast, where ~2.5 km^3 of the 43 km^3 edifice was mobilized. Pre- and post-eruption edifice bounds and calculated edifice centroids are shown on each panel for comparison. The pre-eruption edifice centroid was nearly co-located with the pre-eruption summit, and the post-eruption edifice centroid is shifted only 193 m to the SSW. This minor centroid change is a consequence of only a relatively small part of the overall edifice volume being mobilized during the 1980 events. Elevation and lateral scales are equal for both panels. Pre-eruptive topography was accessed from http://gis.ess.washington.edu/data/raster/thirtymeter/mtsthelens/. Post-eruptive topography is from February 2000 SRTM (NASA JPL, 2013).

Supplementary Tables (separate Microsoft Excel file containing data tables in three sheets, available at: https://doi.org/10.7910/DVN/LHD1HY)

Table S1. List of volcanoes and key edifice morphology and magma reservoir parameters in this study ("Table S1_simplified database" sheet)

Table S2. List of volcanoes and full edifice morphology and magma reservoir parameters in this study ("Table S2_full database" sheet)

Table S3. Summary statistics of geophysically inferred magma reservoirs at different volcano types, compositions, and edifice sizes ("Table S3_summary statistics" sheet).

Data Sets (separate .pdf and .kmz files, available at: https://doi.org/10.7910/DVN/LHD1HY)

Data Set S1. A collection of maps (as a PDF) showing edifice bounds and centroids overlain on topographic maps of each volcano in the database.

Data Set S2. Google Earth database of volcanic edifice bounds and geophysically imaged magma reservoirs. This is a Google Earth .kmz file with all volcano edifice bounds and locations of edifice centroids, vents, summits, and magma reservoirs, as well as supporting figure overlays from the literature that were used for mapping magma reservoir locations.